TÉCNICO LISBOA

Coordinated Control of quadcopters for large object positioning

Maria Inês Ribeiro Soares

Thesis to obtain the Master of Science Degree in

Electrical and Computer Engineering

Supervisor(s): Prof. João Manuel Lage de Miranda Lemos

Prof. Rita Maria Mendes de Almeida Correia da Cunha

Examination Committee

Chairperson: Prof. João Fernando Cardoso Silva Sequeira

Supervisor: Prof. Rita Maria Mendes de Almeida Correia da Cunha

Member of the Committee: Prof. Bruno João Nogueira Guerreiro

September 2021

TÉCNICO LISBOA

Declaração/ Statement

Declaro que o presente documento é um trabalho original da minha autoria e que cumpre todos os requisitos do Código de Conduta e Boas Práticas da Universidade de Lisboa.

I declare that this document is an original work of my own and that it fulfills all the requirements of the Code of Conduct and Good Practices of the Universidade de Lisboa.

Nome/Name: Maria Inês Rijo Ribeiro Soares

Nº de aluno:/Student number: 84130

Lisboa, 8/9/2021

Assinatura/Signature: Maria Inês Rijo Ribeiro Soares

Acknowledgments

Throughout the writing of this thesis, several people played an important role in the guidance and encouragement they gave me.

First, I want to acknowledge my family, whose support was essential for me. In particular, I want to acknowledge my sister Elisa and Tiago for always supporting me and believing in my abilities more than I do.

Secondly, I want to thank my supervisors, Professor Rita Cunha and Professor João Miranda Lemos for working with me continuously, every week, giving me constructive criticism, advice and for sharing their knowledge with me. Thanks to you, I have evolved a lot and I am very grateful for the time you took to help me. I also want to thank all the teachers who have passed through my life over these 5 years, who have given me essential tools for critical thinking and that contributed to my knowledge.

Finally, I leave a word to my friends who accompanied me in my academic life at Instituto Superior Técnico. Without you this journey would not have been so memorable. To all, thank you!

This work has been done in the framework of project HARMONY, funded by Portugal 2020 through FCT (Fundação para a Ciência e a Tecnologia), Portugal, under contract AAC nº2/SAICT/2017 - 031411 and supported by POR Lisboa - LISBOA-01-0145-FEDER-031411 and project REPLACE also funded by Portugal 2020 through FCT, under contract PTDC/EEI-AUT/32107/2017, supported by POR Lisboa - LISBOA-01-0145-FEDER-032107.

Abstract

In recent years, unmanned aerial vehicles such as drones have been gaining prominence as alternatives for performing several tasks. Although this type of vehicle has undergone several improvements in a short period of time, in most cases its flight time is not yet long enough to allow certain missions to run only with the autonomy of a single vehicle. Additionally, the transport of large objects in general is not feasible with a single drone. It is therefore necessary to consider the intervention of two or more vehicles.

In this context, this study aims to develop a controller for a multi-drone system, in order to allow the transport of objects that cannot be handled by just one vehicle. To this end, different models were analyzed in order to characterize several scenarios of object transport, including a 2D scenario with two birotors transporting a load and a 3D scenario with two quadrotors transporting a load restricted to keep a horizontal configuration. Furthermore, the question of drone autonomy and the replacement of vehicles was addressed, considering a mission scenario that goes beyond the capabilities of the energy stored in a single vehicle and requires drone replacement to be performed. The problem addressed involved optimizing the time instants for executing the take-off of a replacement drone and determining the meeting point between the two drones, taking energy consumption into account. The control strategy used for the development of this controller is based on non-linear model predictive control (NMPC) algorithms.

Backed with simulation results, it is shown that the cooperation of vehicles for the purpose of carrying out the transport task is feasible, under certain assumptions. Additionally, the vehicle replacement problem is implemented and tested, based on an energy consumption model defined for each vehicle involved in the transport task. The numerical simulations were created in MATLAB resorting to the solvers fmincon and ode45 and its results verify the effectiveness of the proposed control strategies for both problems.

Keywords: Drones, Model Predictive control, Multi-drone system, Replacement of vehicles.

Resumo

Nos últimos anos, os veículos aéreos não tripulados tal como os drones, têm ganho destaque como alternativas para a realização de diversas tarefas. Embora este tipo de veículo tenha sofrido várias melhorias num curto período de tempo, na maioria dos casos o seu tempo de voo ainda não é longo o suficiente de forma a permitir que certas missões sejam executadas com a autonomia de um único veículo. Além disso, o transporte de objetos de grandes dimensões em geral não é exequível de ser realizado com um único drone. É portanto necessário considerar a intervenção de dois ou mais veículos.

Neste contexto, este estudo tem como objetivo desenvolver um controlador para um sistema multi-drone, de forma a permitir o transporte de objetos que não podem ser manipulados por apenas um veículo. Para este fim, diferentes modelos foram analisados de forma a caracterizar diversos cenários de transporte de objetos, incluindo um cenário 2D com dois birotores que transportam uma carga e um cenário 3D com dois quadrotores que transportam uma carga restrita de maneira a manter uma configuração horizontal. Além disso, foi abordada a questão de autonomia dos drones e a substituição de veículos, considerando um cenário de missão que vai além das capacidades da energia armazenada num único veículo e requer a substituição de um drone. O problema abordado envolveu a otimização dos instantes de tempo para execução da descolagem de um drone substituto e a determinação do ponto de encontro entre os dois drones, tendo em consideração o seu consumo de energia. A estratégia de controlo utilizada para o desenvolvimento deste controlador é baseada em algoritmos de controlo preditivo não linear (NMPC).

Através de resultados de simulações, mostra-se que a cooperação de veículos com o propósito de realizar a tarefa de transporte é viável, sob certos pressupostos. Adicionalmente, o problema de substituição de veículos é implementado e testado, com base num modelo de consumo de energia definido para cada veículo envolvido na tarefa de transporte. As simulações numéricas foram criadas no MATLAB, recorrendo aos solvers fmincon e ode45 e os seus resultados verificam a eficácia das estratégias de controlo propostas para ambos os problemas.

Palavras-chave: Drones, Controlo preditivo, Sistema multi-drone, Substituição de veículos.

Contents

List of Tables

List of Figures

Chapter 1

Introduction

1.1 Motivation

Although initially conceived for military purposes, drones have nowadays a wide spectrum of applications which has resulted in their rapid development and adaptation to various scenarios and environments to carry out challenging missions.

There are many fields where the presence of these vehicles can bring added-value. One such example is agriculture. Applications in these sector pose more and more challenges, in particular due to motivations related to climate change. In fact, according to FAO[1] and ITU[2], the world population and food production worldwide will have to increase by 70% by 2050 [13]. Drones can greatly reduce the costs of this action through analysis of soils and fields, crop monitoring, aerial planting and irrigation, among others. [12].

Another area where drones can make a difference is multimedia and film applications. Most films have motion sequences whose image needs to be obtained from different angles, which requires installing multiple cameras in different places or adopting a better alternative: using drones. The performance of these vehicles has increased more and more in this area. However, there are still several challenges such as estimating the actor's position, understanding the context of the scene at an artistic level and operating in scenarios without prior information [14].

The versatility of drones in various contexts has increased interest of researchers in exploring the cooperation of these vehicles in order to solve increasingly complex problems. One of these problems is the transport of large objects. In this context, the present study addresses the situation in which a single vehicle cannot handle a large object and, therefore, the need for cooperation between two or more of these vehicles arises. In this scenario, the problem of drone autonomy will also be addressed so that the mission to be carried out is not interrupted.

[1] Food and Agriculture Organization of the United Nations.
[2] International Telecommunication Union

1.2 State of the Art

Since the late 1980s, model predictive control (MPC) has gained prominence as a control design technique due to its distinct ability to incorporate optimization features and constraints. In particular, the appearance of nonlinear predictive control allowed the development of controllers that deal with nonlinearities present in the dynamics of models, that further extended the scope of MPC applications. In fact, this control strategy can be very efficient in controlling systems such as UAVs as seen in [15], where the authors control a quadcopter using this technique, taking into account restrictions to the problem.

As already mentioned, nowadays there are countless areas where drones can intervene in order to simplify and solve problems. In fact, recently, the assignment of cooperative tasks for multi-drone systems has been extensively studied, with different models and algorithms already proposed. One such example is [17], that presents a multi-drone approach to autonomous cinematography planning where an architecture based on a cooperative team is proposed. This new application raises a series of challenges since vehicles are expected to make decisions in real time and to capture images autonomously, while following guidelines present in typical filming of cinematography rules.

This thesis explores another application of multi-drone systems: the transport of objects large enough that require two or more vehicles to perform the task. This situation was addressed in [18], where the authors present a configuration where a set of drones are rigidly connected to the object to be transported. In the present study, a different approach is adopted that considers a configuration where each drone is connected to the object by an articulation, which allows the total mobility of the vehicle, that moves with the usual four degrees of freedom. Additionally, a centralized control approach is considered, in contrast to the one presented in [18], which is implemented through a decentralized controller.

It is also important to address the problem of drone autonomy, especially in missions that depend on more than one vehicle, since its battery is a limited resource. There are several solutions for extending a UAV mission. The approach considered in this work is based on the replacement of vehicles in order to ensure the continuity of the assigned task. A relevant article that addresses this issue is [9], applied to the area of structural inspection. For this purpose, the authors propose a continuity-of-service algorithm based on an extension of the MAVLink protocol that implements the replacement of vehicles automatically, through messages and commands that allow communication between drones.

1.3 Objectives

The focus of this thesis is to develop and test a controller for a multi-drone system that allows the transportation of large objects that cannot be transported by a single vehicle. The control strategy used in the development of this controller is based on a non-linear approach to predictive control (NMPC). Throughout this thesis, increasingly complex scenarios have been considered for the cooperation of vehicles, which is reflected in the examples presented. In short, the main objectives of this work are to implement a controller capable of:

- solving the problem of transporting large objects by a multi-drone system and, for that purpose, to

generate optimal trajectories.

- solving the vehicle replacement problem by taking into consideration energy consumption and optimizing the time instants for executing the take-off of a replacement drone and determining the meeting point between the two drones.

1.4 Contributions

The main contributions of this study are algorithms based on nonlinear predictive control that allow vehicle motion control and the replacement of vehicles and also the analysis of the performance of the algorithm based on the study of the simulation.

1.5 Thesis Outline

This report explores the themes previously presented, where different models are studied and the simulations of the respective implementations are presented. This work is divided as follows

- **Chapter 1** introduces the problem, explaining the motivation behind it, where a review of state of the art methods is done. The objectives intended for this work are also defined, as well as the contributions added by it.
- In **chapter 2**, the formulation of the problem is explained in detail. The configuration of the system, its limitations and the assumptions of the problem are addressed. It also refers to the study of the models that will be analyzed in order to address the central problem of the dissertation and, for that purpose, the methods that will be used throughout the work.
- In **chapter 3**, four different systems are modeled, where their limitations and assumptions are explained, based on the study of the bi-rotor and the quadcopter.
- **Chapter 4** presents the problem of control of the system composed of two bi-rotors and a bar. In this chapter, the optimization variables, the cost function to be minimized and the optimization problem are defined. Simulations are also carried out in order to ascertain the performance of the system.
- **Chapter 5** addresses the development of the control strategy for the central problem of this work: the transportation of a bar through the cooperation of two drones. In this Chapter, the optimization problem is defined and simulations of different maneuvers are carried out in order to assess the robustness of the controller developed for this system. The drone autonomy problem is also analyzed and solved through a vehicle replacement strategy. For this purpose, two different situations are presented that portray the replacement of vehicles in a transport task.
- **Chapter 6** addresses the problem of vehicle replacement, in a context where a drone performs a transport task and there is a need for intervention by another vehicle since the first drone does not

have the autonomy to complete the task until the end. In this context, vehicle energy consumption models are defined in order to address and solve the problem in question.

- Finally, in **chapter 7**, the findings of this study are discussed and recommendations are made for future improvements in the results obtained.

Chapter 2

Problem Statement

This chapter addresses the formulation of the central problem of this work, in detail. The configuration of the system in question, the assumptions considered and its limitations are explained. Also mentioned are the models studied in the dissertation and its respective optimization problems addressed before analyzing this problem, in order to carry out a study with increasing complexity.

The central problem of this dissertation is the transportation of large objects by a multi-drone system. This system is composed of two quadcopters and a bar. The drones and the bar are connected through spherical joints that allow both vehicles to move with freedom of movement, without compromising the transport of this object. Fig. 2.1 shows this configuration, where the joints are represented by two circles, connecting each vehicle to the object.

Figure 2.1: Configuration of the quadcopter bar system.

For this problem, the following premises are assumed

1. The movement of the system in two dimensions (x and y) is decoupled from the longitudinal movement. In other words, these two separate movements are considered since the system moves at $z = 0$, where the three rotation angles of drone i (ϕ_i, θ_i, ψ_i, $i = 1, 2$.) are considered as the angle of the bar around the z axis, ψ_b.
2. The bar has a defined length c and negligible width and height.
3. The center of mass of the system coincides with the center of mass of the bar.
4. Both vehicles have autonomy to carry out the task of transport until the end.

Throughout the work, an analysis of 4 different models is carried out, with increasing complexity, where the last situation addressed corresponds to the quadcopter bar system described in this section. First,

the planar model of the drone is analyzed and, then, the study of a system composed by two planar drones that carry a bar is done. Finally, the quadcopter model is explored, in order to proceed with the study of this final system.

Additionally, a control strategy was implemented for the bi-rotor bar system and, subsequently, for the quadcopter bar system. In both cases, the control strategy is based on non-linear predictive control. The objective in controlling these systems is to successfully complete the task of transporting the bar, without compromising the stability while generating optimal trajectories.

At the end of this work, a different scenario of object transport is approached, taking into account the autonomy of each vehicle. It is considered a scenario in which a drone is capable of transporting the bar but it does not have the autonomy to carry out the assigned task until the end, which leads to the need for the intervention of another vehicle. This example adopts some simplifications such as considering that a single drone is capable of transporting the bar and the disregard of charging stations, among others.

Chapter 3

System Modeling

The first requirement for controlling a given system based on a control strategy is to make a reliable description by delineating a model. In order to achieve the final objective of this thesis, where the implementation of a system consisting of multiple quadcopters is carried out, two isolated models were studied: first the bi-rotor and then the quadcopter. Subsequently, scenarios for transporting objects that cannot be transported by just one vehicle are described, first for a system formed by bi-rotors and then for a system composed of quadcopters.

In Section 3.1, the planar drone model is described and its dynamics are defined using the Euler-Lagrange equations. Section 3.2 describes the transport of a bar by two bi-rotors. The dynamics of this system is also defined as a solution of the Euler-Lagrange equation. Moreover, the forces acting on this system are described in detail. Section 3.3 describes the model that is the basis of this work: the quadcopter. The quadcopter kinematics and actuation are explained as well as the equations that describe its movement. Finally, in Section 3.4, the model of a system composed of quadcopters and a bar is defined. The rotation of the three rigid bodies is analyzed and the dynamics of the system are defined.

3.1 Bi-rotor model

A bi-rotor is a planar drone with two rotors. In this section, a vehicle similar to that shown in Fig. 3.1 is studied. In this example, it is considered that its mass, m, is concentrated in a material point located in the center of mass of the vehicle and takes the value $m = 1\ kg$. The bi-rotor moves with an angle θ in relation to the horizontal plane, known as its pitch angle.

Additionally, it is remarked that b corresponds to the distance between each rotor and the center of mass of the UAV, F_g corresponds to the force of gravity, f_1 and f_2 correspond to the forces generated by each rotor of the vehicle, and $f = f_1 + f_2$ corresponds to the total thrust exerted by the vehicle rotors.

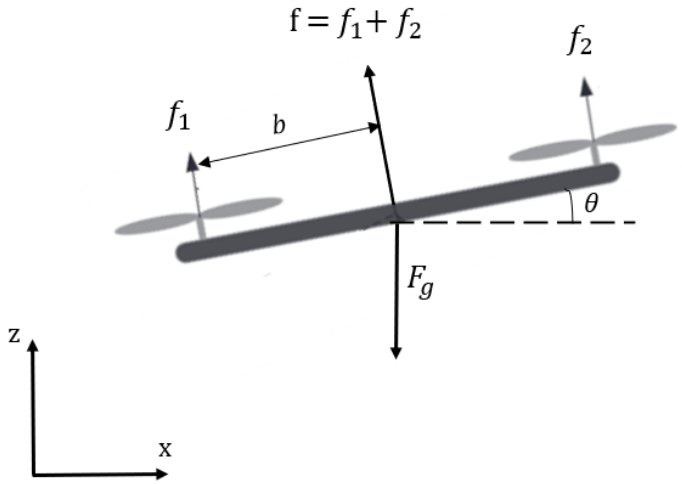

Figure 3.1: Bi-rotor model, adapted from [3].

Euler-Lagrange equations

In relatively simple systems it is possible to define its dynamics analytically through the solutions that result from the Euler-Lagrange equations, satisfied by the generalized coordinates of the system. The generalized coordinates of this system fully describe it and are as follows

$$q = \begin{bmatrix} x & z & \theta \end{bmatrix}, ^T \tag{3.1}$$

composed by the position of the bi-rotor (x and z) and its pitch angle, θ.

The kinetic energy (K) and the potential energy (U) of the system are given by

$$\begin{aligned} K(q, \dot{q}) &= \frac{1}{2} m \dot{x}^2 + \frac{1}{2} m \dot{z}^2 + \frac{1}{2} I \dot{\theta}^2, \\ U(q) &= mgz, \end{aligned} \tag{3.2}$$

where I corresponds to the UAV moment of inertia.

Considering the Lagrangian function $L = K(q, \dot{q}) - U(q)$, the Euler-Lagrange equation takes the form

$$\frac{\partial}{\partial t}\left(\frac{\partial L}{\partial \dot{q}}\right) - \frac{\partial L}{\partial q} = F, \tag{3.3}$$

where F are the generalized forces that act on the system. In this case, F is a vector whose first two entries correspond to the decomposition of the total thrust force exerted on the bi-rotor, in the x and z directions. Fig. 3.2 shows the decomposition of the total thrust force exerted on the bi-rotor.

As it is observable, the first entry of F is the force $f_x = -f \sin(\theta)$, that acts in the horizontal direction of the planar drone and corresponds to the x component of the total thrust that is exerted on the vehicle. Additionally, its second entry is $f_z = f \cos(\theta)$, that is the force that acts in the vertical direction of the planar drone and corresponds to the y component of the total thrust. Note that the x component is negative as f_x is pointing in the negative direction of the x axis and the y component is positive as f_z

is pointing in the positive direction of the z axis. Finally, the last entry of F is $\tau = b(f_1 - f_2)$, which corresponds to the pitching moment provided by the rotors that acts on the pitch axis of the bi-rotor.

In short, F corresponds to

$$F = \begin{bmatrix} -f\sin(\theta) & f\cos(\theta) & \tau \end{bmatrix}^T.$$

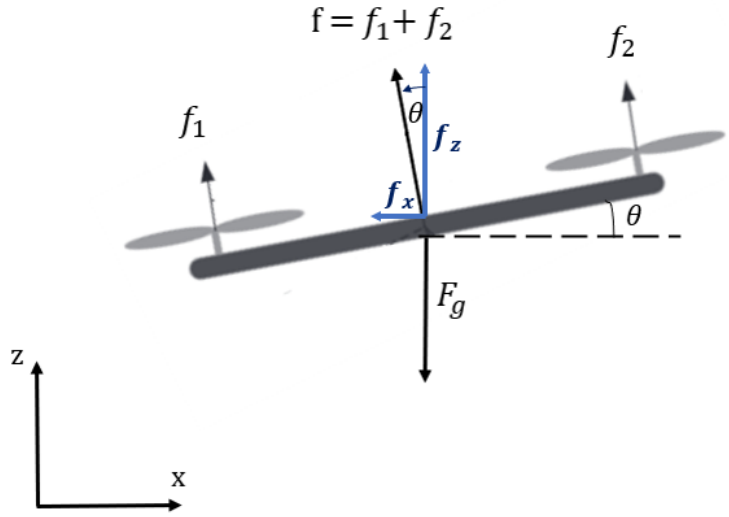

Figure 3.2: Decomposition of the total force exerted on the bi-rotor, adapted from [3].

Finally, the Euler-Lagrange equation can be written as

$$\frac{\partial}{\partial t}\left(\frac{\partial L}{\partial \dot{q}}\right) - \frac{\partial L}{\partial q} = \begin{bmatrix} -f\sin(\theta) \\ f\cos(\theta) \\ \tau \end{bmatrix}. \tag{3.4}$$

Bi-rotor dynamics

Substituting L in (3.4) and solving the equation, the following equations are obtained

$$\begin{aligned} m\ddot{x} &= -f\sin\theta, \\ m\ddot{z} + mg &= f\cos\theta, \\ I\ddot{\theta} &= \tau. \end{aligned} \tag{3.5}$$

The dynamics of the bi-rotor can then be written in the following more compact form

$$\begin{aligned} I\ddot{\theta} &= b(f_1 - f_2), \\ m\begin{bmatrix} \ddot{x} \\ \ddot{z} \end{bmatrix} &= \begin{bmatrix} 0 \\ -mg \end{bmatrix} + R(\theta)\begin{bmatrix} 0 \\ f_1 + f_2. \end{bmatrix}, \end{aligned} \tag{3.6}$$

where $R(\theta)$ represents the rotation matrix, given by

$$R(\theta) = \begin{bmatrix} cos(\theta) & -sin(\theta) \\ sin(\theta) & cos(\theta) \end{bmatrix}. \tag{3.7}$$

3.2 Bi-rotor bar model

Consider two bi-rotors, with masses m_1 and m_2, that cooperate in order to carry a bar of length c and negligible width. The bar is articulated to each vehicle through spherical joints. The configuration of this articulation allows both vehicles to move with freedom of movement.

Fig. 3.3 shows the bi-rotor bar system, where the position of each rigid body is defined in the inertial frame, $\{I\}$, as follows

$$\begin{aligned} p^I_{D_1} &= \begin{bmatrix} x_1 & z_1 \end{bmatrix}^T, \\ p^I_{D_2} &= \begin{bmatrix} x_2 & z_2 \end{bmatrix}^T, \\ p^I_{bar} &= \begin{bmatrix} x_b & z_b \end{bmatrix}^T. \end{aligned} \tag{3.8}$$

Additionally, it is possible to observe the pitch angles of each bi-rotor, θ_1 and θ_2. Note that, each time the bar is not parallel to the horizontal plane, it assumes a rotation angle, called θ_b.

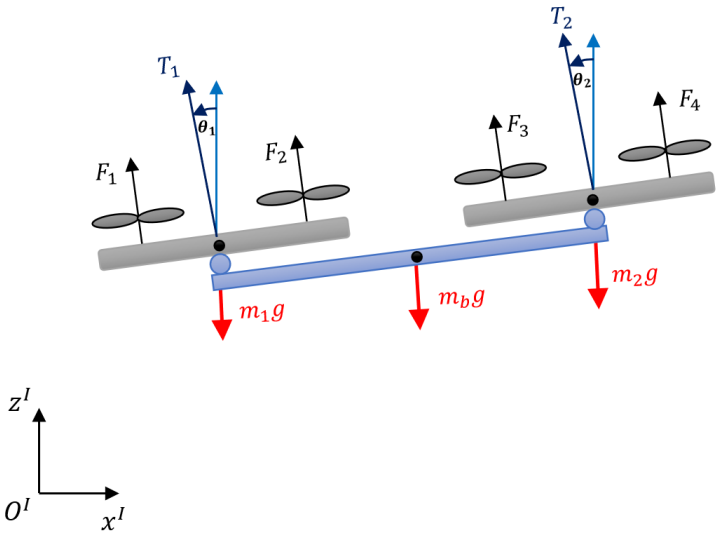

Figure 3.3: Bi-rotor-bar model.

Furthermore, the forces generated by each rotor (F_1, F_2, F_3, F_4) and the total thrust force exerted on each vehicle are represented, which are defined for each bi-rotor as follows

$$\begin{aligned} T_1 &= F_1 + F_2, \\ T_2 &= F_3 + F_4. \end{aligned} \tag{3.9}$$

Additionally, the pitch moments derived by the rotors of each UAV are given by

$$\begin{aligned} \tau_1 &= b(F_1 - F_2), \\ \tau_2 &= b(F_3 - F_4). \end{aligned} \tag{3.10}$$

The parameters used in the modeling of this system are defined in Table 3.1.

	Symbol	Value
Mass of bi-rotor body [kg]	m_1,m_2	1
Mass of bar [kg]	m_b	0.5
Bar length [m]	c	1

Table 3.1: Parameters applied for the bi-rotor bar system.

Euler-Lagrange equations

The definition of the dynamics of this system is the result of the solution of the Euler-Lagrange equation, satisfied by the generalized coordinates of the system. In this example, it is assumed that the center of mass of the system coincides with the center of mass of the bar. Thus, this system is described in its entirety through the following generalized coordinates

$$q = \begin{bmatrix} x_b & z_b & \theta_1 & \theta_2 & \theta_b \end{bmatrix}^T, \tag{3.11}$$

that are composed by the position of the bar (x_b and z_b), the pitch angles of each vehicle (θ_1 and θ_2) and the rotation angle of the bar, θ_b, performed in the xz-plane.

In order to define the Euler-Lagrange equation it is necessary to first define the potential and kinetic energies of the system. Thus, the kinetic energy (K) and the potential energy (U) of the system are given by

$$\begin{aligned} K(q,\dot{q}) &= \frac{1}{2}m_b\dot{x}_b^2 + \frac{1}{2}m_b\dot{z}_b^2 + \frac{1}{2}m_1\dot{x}_1^2 + \frac{1}{2}m_1\dot{z}_1^2 + \frac{1}{2}m_2\dot{x}_2^2 + \frac{1}{2}m_2\dot{z}_2^2 + \frac{1}{2}I_b\dot{\theta}_b^2 + \frac{1}{2}I_1\dot{\theta}_1^2 + \frac{1}{2}I_2\dot{\theta}_2^2, \\ U(q) &= m_b g z_b + m_1 g z_1 + m_2 g z_2, \end{aligned} \tag{3.12}$$

where I_b corresponds to the moment of inertia of the bar and I_1 and I_2 correspond to the moments of inertia of each vehicle. Since both vehicles have the same mass, the following simplification is adopted: $m_1 = m_2 = m$.

It is remarked that the positions of both bi-rotors, $p^I_{D_1}$ and $p^I_{D_2}$, can be defined through the bar generalized coordinates, x_b, z_b and θ_b, and are given by

$$\begin{aligned} x_1 &= x_b - \frac{c}{2}\cos(\theta_b), \\ z_1 &= z_b - \frac{c}{2}\sin(\theta_b), \\ x_2 &= x_b + \frac{c}{2}\cos(\theta_b), \\ z_2 &= z_b + \frac{c}{2}\sin(\theta_b). \end{aligned} \tag{3.13}$$

Moreover, their respective derivatives are

$$\begin{aligned}
\dot{x}_1 &= \dot{x}_b + \frac{c}{2}\dot{\theta}_b \sin(\theta_b), \\
\dot{z}_1 &= \dot{z}_b - \frac{c}{2}\dot{\theta}_b \cos(\theta_b), \\
\dot{x}_2 &= \dot{x}_b - \frac{c}{2}\dot{\theta}_b \sin(\theta_b), \\
\dot{z}_2 &= \dot{z}_b + \frac{c}{2}\dot{\theta}_b \cos(\theta_b).
\end{aligned} \tag{3.14}$$

The Lagrangian function, $L = K(q, \dot{q}) - U(q)$, must be written taking into account the generalized coordinates defined in (3.11). For this purpose, the linear velocities of both vehicles ($\dot{x}_1$, $\dot{z}_1$, $\dot{x}_2$ and $\dot{z}_2$) are replaced by its equivalent expressions defined in (3.14). Hence, the following Lagrangian function is obtained

$$L = (\frac{1}{2}m_b + m)\dot{x}_b^2 + (\frac{1}{2}m_b + m)\dot{z}_b^2 + m\frac{c^2}{4}\dot{\theta}_b + \frac{1}{2}I_b\dot{\theta_b}^2 + \frac{1}{2}I_1\dot{\theta_1}^2 + \frac{1}{2}I_2\dot{\theta_2}^2 - (m_b + 2m)gz_b \tag{3.15}$$

The dynamics of the bi-rotor are defined through the Euler-Lagrange equation, which is given by

$$\frac{\partial}{\partial t}(\frac{\partial L}{\partial \dot{q}}) - \frac{\partial L}{\partial q} = F, \tag{3.16}$$

where F are the generalized forces that act on the system. In order to define vector F, it is required to decompose the forces present in this system. Fig. 3.4 shows the decomposition of the total thrust force exerted on each bi-rotor, T_1 and T_2, in the x and z directions.

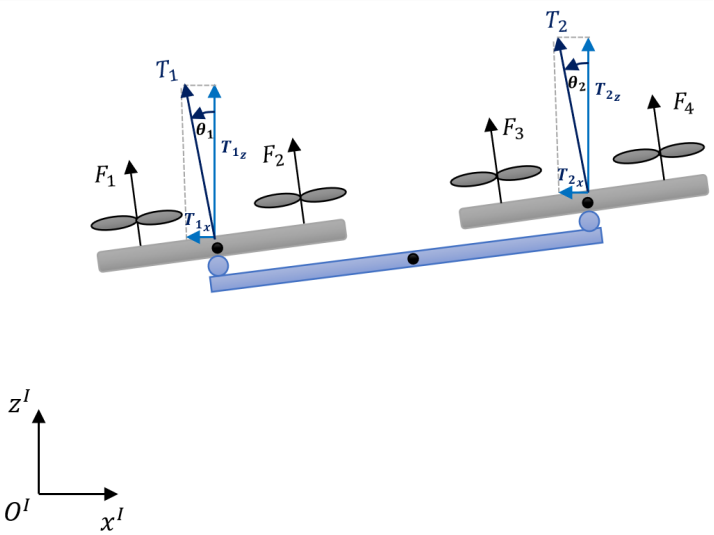

Figure 3.4: Decomposition of the total thrust of both vehicles.

Both components of the forces T_1 and T_2, are defined in a similar way, using trigonometry. The

decomposition of T_1 and T_2 is given by

$$
\begin{aligned}
T_{1_x} &= -T_1 \sin(\theta_1), \\
T_{1_z} &= T_1 \cos(\theta_1), \\
T_{2_x} &= -T_2 \sin(\theta_2), \\
T_{2_z} &= T_2 \cos(\theta_2).
\end{aligned}
$$

Note that the x components are negative as T_{1_x} and T_{2_x} are pointing in the negative direction of the x axis and the z components are positive as T_{1_z} and T_{2_z} are pointing in the positive direction of the z axis.

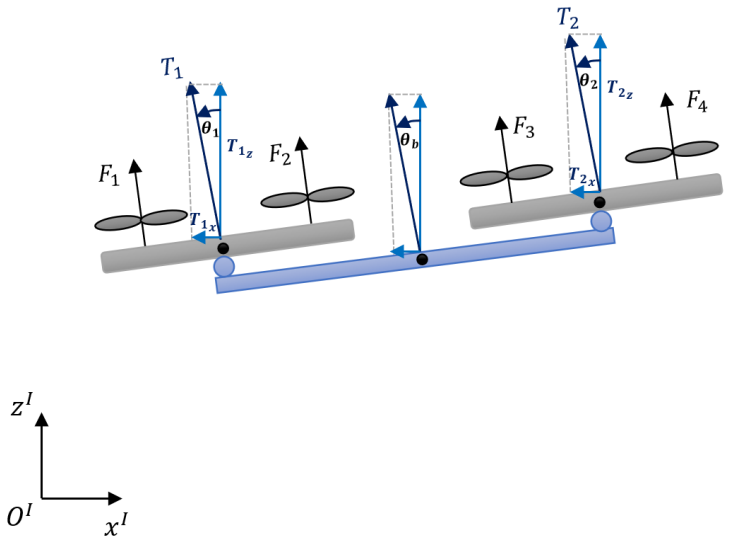

Figure 3.5: Decomposition of the total force exerted on the bar by both vehicles.

Fig. 3.5 shows the components in the x and z directions of the total thrust forces exerted on both vehicles and also T_b, which corresponds to the total force exerted on the bar by the two planar drones. T_b takes into account the components in x and z of T_1 and T_2.

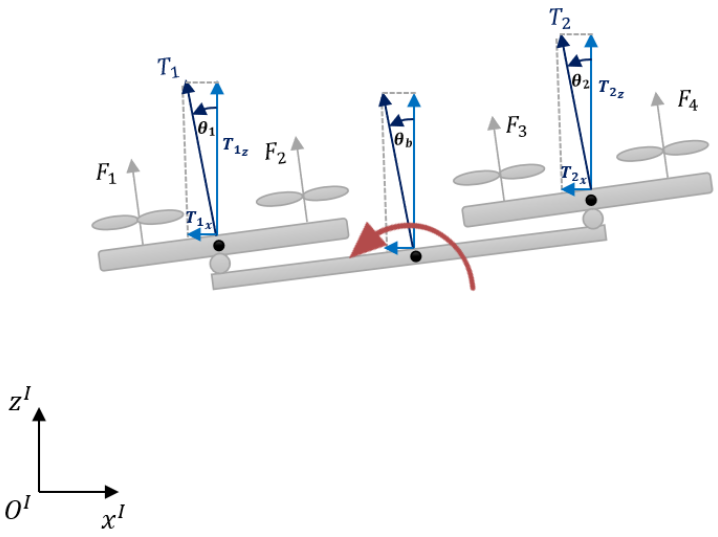

Figure 3.6: Decomposition of the total force exerted on the bar by both vehicles.

In Fig. 3.6, the positive direction of rotation of the system is represented in red, which corresponds to a counterclockwise rotation. Taking into account the direction of this rotation, T_b is calculated as follows

$$\begin{aligned} T_b &= T_2\cos(\theta_2)\cos(\theta_b) + T_2(-\sin(\theta_2))(-\sin(\theta_b)) - T_1\cos(\theta_1)\cos(\theta_b) + T_1(-\sin(\theta_1))(-\sin(\theta_b)) \Leftrightarrow \\ &\Leftrightarrow T_b = T_2\cos(\theta_2)\cos(\theta_b) + T_2\sin(\theta_2)\sin(\theta_b) - T_1\cos(\theta_1)\cos(\theta_b) + T_1\sin(\theta_1)\sin(\theta_b) \Leftrightarrow \\ &\Leftrightarrow T_b = T_2[\cos(\theta_2)\cos(\theta_b) + \sin(\theta_2)\sin(\theta_b)] - T_1[\cos(\theta_1)\cos(\theta_b) + \sin(\theta_1)\sin(\theta_b)]. \end{aligned} \tag{3.17}$$

Using the trigonometric form $\cos(a-b) = \cos(a)\cos(b) + \sin(a)\sin(b)$, T_b can be written in the following more compact way

$$T_b = T_2\cos(\theta_2 - \theta_b) - T_1\cos(\theta_1 - \theta_b). \tag{3.18}$$

The inputs of vector F can now be defined. The first entry of F corresponds to the sum of the forces of both vehicles in the x direction and its second entry corresponds to the sum of the forces of both vehicles in the z direction. The third and fourth entries of F correspond to the pitching moment of each vehicle and, finally, its last entry corresponds to T_b.

In short, F is given by

$$F = \begin{bmatrix} -T_1\sin(\theta_1) - T_2\sin(\theta_2) & T_1\cos(\theta_1) + T_2\cos(\theta_2) & \tau_1 & \tau_2 & T_2\cos(\theta_2 - \theta_b) - T_1\cos(\theta_1 - \theta_b) \end{bmatrix}^T.$$

Finally, the Euler-Lagrange equation is the following

$$\frac{\partial}{\partial t}(\frac{\partial L}{\partial \dot{q}}) - \frac{\partial L}{\partial q} = \begin{bmatrix} -T_1 \sin(\theta_1) - T_2 \sin(\theta_2) \\ T_1 \cos(\theta_1) + T_2 \cos(\theta_2) \\ \tau_1 \\ \tau_2 \\ T_2 \cos(\theta_2 - \theta_b) - T_1 \cos(\theta_1 - \theta_b) \end{bmatrix}. \tag{3.19}$$

System dynamics

The equations of motion of the system derived from (3.19) are given by

$$\begin{aligned} &I_1 \ddot{\theta_1} = \tau_1, \\ &I_2 \ddot{\theta_2} = \tau_2, \\ &(I_b + m\frac{c^2}{2})\ddot{\theta_b} = T_2 \cos(\theta_2 - \theta_b) - T_1 \cos(\theta_1 - \theta_b), \\ &(2m + m_b)\ddot{x_b} = -T_1 \sin\theta_1 - T_2 \sin\theta_2, \\ &(2m + m_b)\ddot{z_b} + (2m + m_b)g = T_1 \cos\theta_1 + T_2 \cos\theta_2. \end{aligned} \tag{3.20}$$

The dynamics of the bi-rotor bar system can be written in the following more compact form

$$\begin{aligned} &\ddot{\theta}_1 = \frac{\tau_1}{I_1}, \\ &\ddot{\theta}_2 = \frac{\tau_2}{I_2}, \\ &\ddot{\theta}_b = \frac{T_2 \cos(\theta_2 - \theta_b) - T_1 \cos(\theta_1 - \theta_b)}{I_b + m\frac{c^2}{2}}, \\ &(2m + m_b) \begin{bmatrix} \ddot{x}_b \\ \ddot{z}_b \end{bmatrix} = \begin{bmatrix} 0 \\ -(2m + m_b)g \end{bmatrix} + R(\theta_1) \begin{bmatrix} 0 \\ T_1 \end{bmatrix} + R(\theta_2) \begin{bmatrix} 0 \\ T_2 \end{bmatrix}, \end{aligned} \tag{3.21}$$

where $R(\theta_1)$ and $R(\theta_2)$ represent the following rotation matrices

$$R(\theta_1) = \begin{bmatrix} cos(\theta_1) & -sin(\theta_1) \\ sin(\theta_1) & cos(\theta_1) \end{bmatrix}, \qquad R(\theta_2) = \begin{bmatrix} cos(\theta_2) & -sin(\theta_2) \\ sin(\theta_2) & cos(\theta_2) \end{bmatrix}. \tag{3.22}$$

3.3 Quadcopter model

A quadcopter is a three-dimensional drone with four rotors. The model of the quadcopter is defined as a rigid body with four degrees of freedom (DOF) in free flight: three DOF with respect to attitude and one DOF with respect to the total thrust force applied to the vehicle.

The position and orientation of a quadcopter are described through two coordinate frames: an inertial frame, $\{I\}$, which is fixed to the Earth, and a body frame, $\{B\}$, which is fixed to the center of mass of the UAV, both represented in Fig. 3.7. In $\{I\}$, the unit vectors $\{e_1, e_2, e_3\}$ match the x, y and z axes, respectively.

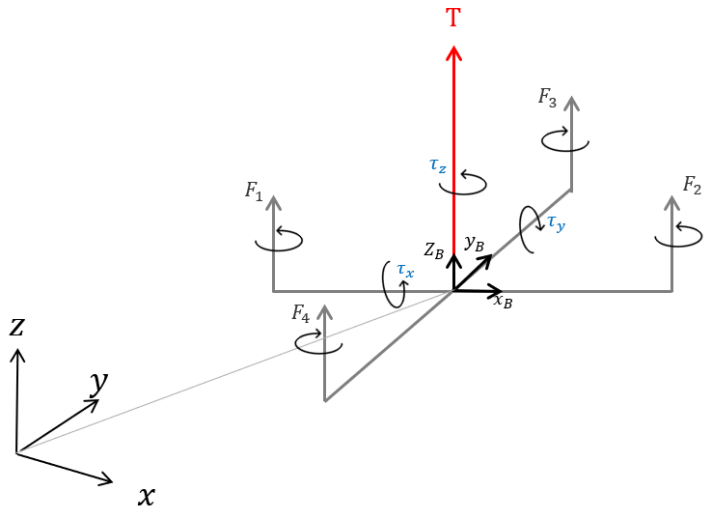

Figure 3.7: Coordinate systems and the forces and moments generated by the quadrotor rotors.

Kinematics

The position and velocity of the quadcopter is denoted in the inertial frame by

$$p^I = p = \begin{bmatrix} x & y & z \end{bmatrix}^T,$$
$$\dot{p} = \begin{bmatrix} \dot{x} & \dot{y} & \dot{z} \end{bmatrix}^T.$$

The vehicle orientation is described by its angles of rotation, the $Z-Y-X$ Euler angles, and are given by

$$\Theta = \begin{bmatrix} \phi & \theta & \psi \end{bmatrix}^T,$$

which correspond to roll, pitch and yaw rotations, respectively [5]. The transformation from the body frame to the inertial frame is given by three consecutive rotations around the three defined axes, using the $Z-Y-X$ Euler angles convention. The rotation matrix between the body frame and the inertial

frame is defined, through the referred rotations.

$$
\begin{aligned}
&R_B^I = R_z(\psi)R_y(\theta)R_x(\phi) = \\
&= \begin{bmatrix} \cos\psi & -\sin\psi & 0 \\ \sin\psi & \cos\psi & 0 \\ 0 & 0 & 1 \end{bmatrix} \begin{bmatrix} \cos\theta & 0 & \sin\theta \\ 0 & 1 & 0 \\ -\sin\theta & 0 & \cos\theta \end{bmatrix} \begin{bmatrix} 1 & 0 & 0 \\ 0 & \cos\phi & -\sin\phi \\ 0 & \sin\phi & \cos\phi \end{bmatrix} = \\
&= \begin{bmatrix} \cos\psi\cos\theta & \cos\psi\sin\theta\sin\phi - \sin\psi\cos\phi & \cos\psi\sin\theta\cos\phi + \sin\psi\sin\phi \\ \sin\psi\cos\theta & \sin\psi\sin\theta\sin\phi + \cos\psi\cos\phi & \sin\psi\sin\theta\cos\phi - \cos\psi\sin\phi \\ -\sin\theta & \cos\theta\sin\phi & \cos\theta\cos\phi \end{bmatrix}.
\end{aligned} \tag{3.23}
$$

It is relevant to note that the linear velocities of the quadcopter, given by

$$\dot{p} = \begin{bmatrix} \dot{x} & \dot{y} & \dot{z} \end{bmatrix}^T,$$

can also be transformed, in order to be expressed in the body reference, as follows

$$v^B = \begin{bmatrix} v_x & v_y & v_z \end{bmatrix}^T.$$

This transformation can be synthesized through the following equation

$$v^B = (R_B^I)^T \dot{p}. \tag{3.24}$$

Similarly, the angular velocities of the quadcopter expressed in $\{I\}$, given by

$$\dot{\Theta} = \begin{bmatrix} \dot{\phi} & \dot{\theta} & \dot{\psi} \end{bmatrix}^T,$$

can be expressed in $\{B\}$, resulting in the following angular velocities

$$w^B = \begin{bmatrix} w_x & w_y & w_z \end{bmatrix}^T.$$

This transformation can be written in a compact form, given by

$$w^B = \begin{bmatrix} 1 & 0 & -\sin\theta \\ 0 & \cos\theta & \sin\phi\cos\theta \\ 0 & -\sin\phi & \cos\phi\cos\theta \end{bmatrix} \dot{\Theta}. \tag{3.25}$$

In short, the Translational kinematics of the quadcopter are the inverse form of (3.24) and are given by

$$\dot{p} = R_B^I v^B. \tag{3.26}$$

Additionally, the Rotational kinematics of this vehicle are the inverse form of (3.25) and are the following

$$\dot{\Theta} = \begin{bmatrix} 1 & \sin\phi\tan\theta & \cos\phi\tan\theta \\ 0 & \cos\phi & -\sin\phi \\ 0 & \frac{\sin\phi}{\cos\phi} & \frac{\cos\phi}{\cos\theta} \end{bmatrix} w^B. \tag{3.27}$$

Actuation

Fig. 3.7 shows the four forces $(F_1, F_2, F_3$ and $F_4)$ that are generated by each of the vehicle rotors. The total force exerted on the vehicle, T, and the rolling, τ_x, pitching, τ_y and yawning, τ_z moments, are defined taking into account these forces, as follows

$$\begin{aligned} T &= \sum_{i=1}^{4} F_i = F_1 + F_2 + F_3 + F_4, \\ \tau^B &= \begin{bmatrix} \tau_x \\ \tau_y \\ \tau_z \end{bmatrix} = \begin{bmatrix} d(F_2 - F_3) \\ d(F_1 - F_3) \\ c(F_1 + F_3 - F_2 - F_4) \end{bmatrix}, \end{aligned} \tag{3.28}$$

where d is the distance between each rotor and center of mass of the vehicle and c is a constant coefficient for the induced torque of the motor [4]. Eq.(3.28) can be rewritten in matrix form as follows

$$\begin{bmatrix} T \\ \tau_x \\ \tau_y \\ \tau_z \end{bmatrix} = \begin{bmatrix} 1 & 1 & 1 & 1 \\ 0 & d & -d & 0 \\ d & 0 & -d & 0 \\ c & -c & c & -c \end{bmatrix} \begin{bmatrix} F_1 \\ F_2 \\ F_3 \\ F_4 \end{bmatrix}. \tag{3.29}$$

Quadcopter dynamics

After defining the total force exerted on the vehicle and the torques generated by the quadcopter rotors, the rotational dynamics of the quadcopter can now be defined. The rotational dynamics of the quadcopter are expressed in $\{B\}$ and are given by

$$I\dot{w}^B = -w^B \times Iw^B + \tau^B, \tag{3.30}$$

where the inertial matrix, I, is defined as follows

$$I = \begin{bmatrix} I_{xx} & 0 & 0 \\ 0 & I_{yy} & 0 \\ 0 & 0 & I_{zz} \end{bmatrix}.$$

The terms I_{xx}, I_{yy} and I_{zz} are called inertia products and are defined later in chapter 5, where the control strategy for this system is carried out.

The rotational equation of motion defined in (3.30), can be written in more detail, as follows

$$\begin{bmatrix} I_{xx}\dot{w}_x \\ I_{yy}\dot{w}_y \\ I_{zz}\dot{w}_z \end{bmatrix} = \begin{bmatrix} \tau_x \\ \tau_y \\ \tau_z \end{bmatrix} + \begin{bmatrix} w_y w_z (I_{yy} - Izz) \\ w_x w_z (I_{zz} - Ixx) \\ w_x w_y (I_{xx} - Iyy) \end{bmatrix}. \tag{3.31}$$

Thus, the vector of angular velocities defined in the body reference is then given by

$$\dot{w}^B = I^{-1}(\tau^B - w \times (Iw)) = \begin{bmatrix} \dot{w}_x \\ \dot{w}_y \\ \dot{w}_z \end{bmatrix} = \begin{bmatrix} \tau_x I_{xx}^{-1} \\ \tau_y I_{yy}^{-1} \\ \tau_z I_{zz}^{-1} \end{bmatrix} + \begin{bmatrix} w_y w_z \frac{(I_{yy} - I_{zz})}{I_{xx}} \\ w_x w_z \frac{(I_{zz} - I_{xx})}{I_{yy}} \\ w_x w_y \frac{(I_{xx} - I_{yy})}{I_{zz}} \end{bmatrix}. \tag{3.32}$$

The translational dynamics of the quadcopter are now defined. The translational dynamics of the quadcopter are expressed in $\{I\}$, and are given by

$$m\ddot{p} = -mge_3 + TR_B^I e_3, \tag{3.33}$$

where m is the mass of the quadcopter and g is the force of gravity.

Together, Equations (3.30) and (3.33) completely characterize the movement of this vehicle, as follows

$$\begin{aligned} I\dot{w}^B &= -w^B \times Iw^B + \tau^B, \\ m\ddot{p} &= -mge_3 + TR_B^I e_3. \end{aligned} \tag{3.34}$$

Thus, the state space model is given by

$$\begin{pmatrix} \ddot{x} \\ \ddot{y} \\ \ddot{z} \end{pmatrix} = \begin{pmatrix} 0 \\ 0 \\ -g \end{pmatrix} + \frac{1}{m} \begin{pmatrix} \cos\psi \sin\theta \cos\phi + \sin\psi \sin\phi \\ \sin\psi \sin\theta \cos\phi - \cos\psi \sin\phi \\ \cos\theta \cos\phi \end{pmatrix} T$$
$$\begin{pmatrix} \dot{w}_x \\ \dot{w}_y \\ \dot{wz} \end{pmatrix} = \begin{pmatrix} \frac{1}{I_{xx}} & 0 & 0 \\ 0 & \frac{1}{I_{yy}} & 0 \\ 0 & 0 & \frac{1}{I_{zz}} \end{pmatrix} \begin{pmatrix} \tau_x \\ \tau_y \\ \tau_z \end{pmatrix} + \begin{pmatrix} w_y w_z \frac{I_{yy} - I_{zz}}{I_{xx}} \\ w_x w_z \frac{I_{zz} - I_{xx}}{I_{yy}} \\ w_x w_y \frac{I_{xx} - I_{yy}}{I_{zz}} \end{pmatrix} \tag{3.35}$$

3.4 Quadcopter bar model

Consider a situation in which two quadcopters, with masses m_1 and m_2, carry a bar of length l and of negligible width and height, through spherical joints that allow both vehicles to rotate. That is, the configuration allows both drones to move with freedom of movement.

In Fig. 3.8, a top view of the system is shown, where the references adopted for this problem are represented. The chosen frames are the inertial frame, $\{I\}$, the body frame of each of the drones, $\{B_i\}$ ($i = 1, 2$), and the body frame of the bar, $\{O\}$.

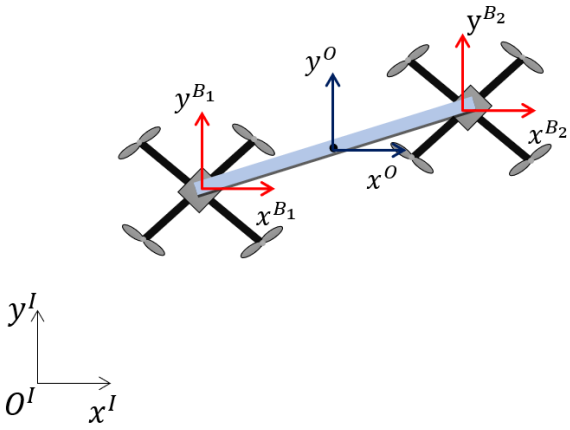

Figure 3.8: System of two quadcopters carrying a bar - top-view.

Kinematics

The positions of the three rigid bodies are given in the inertial frame, respectively, by

$$p_{D_1} = \begin{bmatrix} x_1 \\ y_1 \\ z_1 \end{bmatrix}, \quad p_{D_2} = \begin{bmatrix} x_2 \\ y_2 \\ z_2 \end{bmatrix}, \quad p_{bar} = \begin{bmatrix} x_b \\ y_b \\ z_b \end{bmatrix}. \tag{3.36}$$

In this problem, the system moves strictly at $z = 0$ and only its movement in the xy-plane is analyzed. Thus, the rotation angles considered for each body are $\Theta_1 = \begin{bmatrix} \phi_1 & \theta_1 & \psi_1 \end{bmatrix}^T$, $\Theta_2 = \begin{bmatrix} \phi_2 & \theta_2 & \psi_2 \end{bmatrix}^T$, and ψ_b. Fig. 3.9 shows the Z rotation of the three rigid bodies.

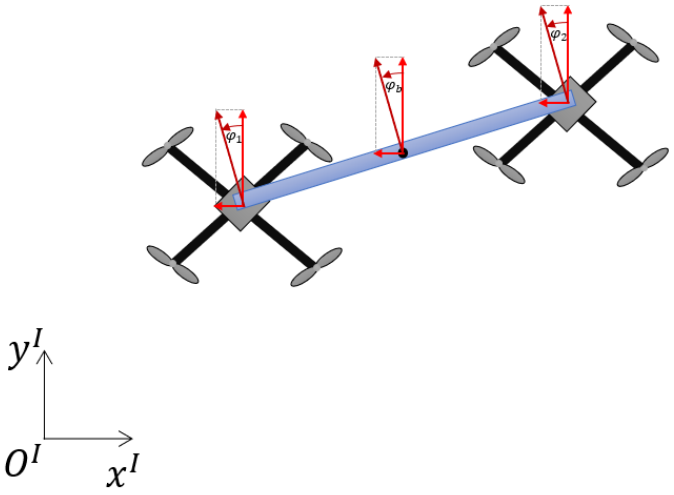

Figure 3.9: System of two quadcopters carrying a bar - top view.

In order to define the dynamics of the system, the rotation matrix R^O_{Bi}, which describes the rotation between $\{B_i\}$ and $\{O\}$, must be described. For this purpose, it is required to first define the rotation matrix, R^I_O, which defines the rotation between the body frame of the bar and the inertial frame. Hence, R^I_O is defined considering the Z rotation of the Euler angles, and its definition is given by

$$R^I_O = \begin{bmatrix} \cos\psi_b & -\sin\psi_b & 0 \\ \sin\psi_b & \cos\psi_b & 0 \\ 0 & 0 & 1 \end{bmatrix}. \tag{3.37}$$

For the sake of simplicity of calculations, a generic body frame, $\{B\}$, is considered. Considering the definition of R^I_B in eq.(3.23), R^O_B is now defined, as follows

$$\begin{aligned} R^O_B &= R^O_I R^I_B = (R^I_O)^T R^I_B = R_z(\psi-\psi_b)R_y(\theta)R_x(\phi) = \\ &= \begin{bmatrix} \cos(\psi_b-\psi)\cos\theta & \sin(\psi_b-\psi)\cos\phi+\cos(\psi_b-\psi)\sin\theta\sin\phi & -\sin(\psi_b-\psi)\sin\phi+\cos(\psi_b-\psi)\sin\theta\cos\phi \\ \sin(\psi-\psi_b)\cos\phi & \cos(\psi_b-\psi)\cos\phi+\sin(\psi-\psi_b)\sin\theta\sin\phi & -\cos(\psi_b-\psi)\sin\phi+\sin(\psi-\psi_b)\sin\theta\cos\phi \\ -\sin\theta & \cos\theta\sin\phi & \cos\theta\cos\phi \end{bmatrix}. \end{aligned} \tag{3.38}$$

Translational dynamics of the system

In this problem, it is assumed that the center of mass of this system coincides with the center of mass of the bar. The bar is considered to be a rigid body, as are both vehicles. Therefore, the translational dynamics of the system are similar to the translational dynamics of the bar, except for the mass and moments of inertia considered. Thus, by analogy with the dynamics of the quadcopters, the dynamics of the system are defined, as follows

$$m_{sys}\ddot{p}^I_b = -m_{sys}ge_3 + T_O, \tag{3.39}$$

where $m_{sys} = m_1 + m_2 + m_b$ corresponds to the total mass of the system.

Additionally, T_O is the total force applied by the vehicles on the bar and is given by

$$\begin{aligned} T_O &= R^I_{B_1} \begin{bmatrix} 0 \\ 0 \\ T_1 \end{bmatrix} + R^I_{B_2} \begin{bmatrix} 0 \\ 0 \\ T_2 \end{bmatrix} = \\ &= \begin{bmatrix} (\cos\psi_1 \sin\theta_1 \cos\phi_1 + \sin\psi_1 \sin\phi_1) T_1 \\ (\sin\psi_1 \sin\theta_1 \cos\phi_1 - \cos\psi_1 \sin\phi_1) T_1 \\ \cos\theta_1 \cos\phi_1 T_1 \end{bmatrix} + \begin{bmatrix} (\cos\psi_2 \sin\theta_2 \cos\phi_2 + \sin\psi_2 \sin\phi_2) T_2 \\ (\sin\psi_2 \sin\theta_2 \cos\phi_2 - \cos\psi_2 \sin\phi_2) T_2 \\ \cos\theta_2 \cos\phi_2 T_2 \end{bmatrix}. \end{aligned} \tag{3.40}$$

Rotational dynamics of the system

Each rigid body has a rotational dynamics that describes its rotation, whose equations are defined in a similar way and are given by

$$\begin{aligned} I\dot{w}^{B_1} &= -w^{B_1} \times I w^{B_1} + \tau^{B_1}, \\ I\dot{w}^{B_2} &= -w^{B_2} \times I w^{B_2} + \tau^{B_2}, \\ I_{sys}\dot{w}^{O} &= -w^{O} \times I_{sys} w^{O} + \tau^{O}, \end{aligned} \tag{3.41}$$

where I_{sys} corresponds to the moment of inertia of the system and I corresponds to the moments of inertia of both UAVs. Both moments of inertia are defined in the following section. τ^{B_1} and τ^{B_2} correspond to the torque exerted on each vehicle and τ^O is the total torque applied by the vehicles on the bar and is defined as follows

$$\begin{aligned} \tau^O &= \begin{bmatrix} L \\ 0 \\ 0 \end{bmatrix} \times R^O_{B_1} \begin{bmatrix} 0 \\ 0 \\ T_1 \end{bmatrix} - \begin{bmatrix} L \\ 0 \\ 0 \end{bmatrix} \times R^O_{B_2} \begin{bmatrix} 0 \\ 0 \\ T_2 \end{bmatrix} = \\ &\begin{bmatrix} 0 \\ -L\cos\theta_1 \cos\phi_1 T_1 + L\cos\theta_2 \cos\phi_2 T_2 \\ (-\cos(\psi_b - \psi_1)\sin\phi_1 + \sin(\psi_1 - \psi_b)\sin\theta_1 \cos\phi_1) T_1 L + (\cos(\psi_b - \psi_2)\sin\phi_2 + \sin(\psi_2 - \psi_b)\sin\theta_2 \cos\phi) T_2 L \end{bmatrix}. \end{aligned} \tag{3.42}$$

System moment of inertia

Table 3.2 shows the values of the parameters considered for this problem. The values of the quadcopter moments of inertia are chosen taking into account the article [8], where experiments were carried out to reach these values.

Symbol	Value
m_1, m_2	$1.12\ kg$
m_b	$0.5\ kg$
I_{xx_1}, I_{xx_2}	$0.0119\ kg.m^2$
I_{yy_1}, I_{yy_2}	$0.0119\ kg.m^2$
I_{zz_1}, I_{zz_2}	$0.0223\ kg.m^2$

Table 3.2: System parameters for simulation.

The moment of inertia of the bar is calculated analytically and is given by

$$\begin{aligned} I_{xx_b} &= \frac{1}{12} m_b (h^2 + w^2) = 0, \\ I_{yy_b} &= \frac{1}{12} m_b (l^2 + h^2) = \frac{1}{12} m_b l^2 \ , \\ I_{zz_b} &= \frac{1}{12} m_b (l^2 + w^2) = \frac{1}{12} m_b l^2, \end{aligned} \tag{3.43}$$

where l corresponds to the length of the bar and w and h are, respectively, the width and height of the bar which in this problem are assumed to be negligible ($w = h = 0$).

The moment of inertia of the total system is defined considering the quadcopters as rigid bodies 1 and 2 and the bar as the third rigid body, whose coordinates are defined in relation to the center of mass of the system, as follows

$$\begin{aligned} body_1 &= (\frac{c}{2}\cos\phi_1, \frac{c}{2}\sin\phi_1, 0) \\ body_2 &= (-\frac{c}{2}\cos\phi_1, -\frac{c}{2}\sin\phi_1, 0) \\ body_3 &= (0, 0, 0) \end{aligned} \tag{3.44}$$

The moment of inertia of the total system is calculated taking into account the definition of the moment of inertia of a rigid composite system, which corresponds to the sum of the moments of inertia of its component subsystems. Thus, the moment of inertia of the total system is defined as follows

$$\begin{aligned} I_X &= \sum_{i=1}^{3} (I_{x_i} + m_i(\bar{y_i}^2 + \bar{z_i}^2)), \\ I_Y &= \sum_{i=1}^{3} (I_{y_i} + m_i(\bar{x_i}^2 + \bar{z_i}^2)), \\ I_Z &= \sum_{i=1}^{3} (I_{z_i} + m_i(\bar{y_i}^2 + \bar{x_i}^2)), \end{aligned} \tag{3.45}$$

where

$$\begin{aligned} \bar{x_i} &= x_i - \bar{X}, \\ \bar{y_i} &= y_i - \bar{Y}, \\ \bar{z_i} &= z_i - \bar{Z}, \end{aligned}$$

and

$$\bar{X} = \frac{\sum_{i=1}^{3} x_i m_i}{\sum_{i=1}^{3} m_i},$$
$$\bar{Y} = \frac{\sum_{i=1}^{3} y_i m_i}{\sum_{i=1}^{3} m_i},$$
$$\bar{Z} = \frac{\sum_{i=1}^{3} z_i m_i}{\sum_{i=1}^{3} m_i}.$$

System dynamics

In short, the total dynamics of the system are composed of the equations (3.39) and (3.41), and are given by

$$\begin{aligned}
\ddot{p}_b^I &= -ge_3 + \frac{T_O}{m_{sys}}, \\
I\dot{w}^{B_1} &= -w^{B_1} \times Iw^{B_1} + \tau^{B_1}, \\
I\dot{w}^{B_2} &= -w^{B_2} \times Iw^{B_2} + \tau^{B_2}, \\
I_{sys}\dot{w}^O &= -w^O \times I_{sys}w^O + \tau^O.
\end{aligned} \tag{3.46}$$

Chapter 4

Control of the bi-rotors bar system

After modeling the system consisting of two bi-rotors and a bar in chapter 3, this chapter focuses on the next step: the problem of control design. In this chapter, the control problem is defined and simulations are presented in order to discuss the robustness of the developed controller.

System dynamics

The dynamics obtained for this system, previously defined in chapter 3, are given by

$$\begin{aligned}
\ddot{\theta}_1 &= \frac{\tau_1}{J_1}, \\
\ddot{\theta}_2 &= \frac{\tau_2}{J_2}, \\
\ddot{\theta}_b &= \frac{T_2\cos(\theta_2-\theta_b) - T_1\cos(\theta_1-\theta_b)}{J_b + m\frac{c^2}{2}}, \\
(2m+m_b)\begin{bmatrix}\ddot{x}_b \\ \ddot{z}_b\end{bmatrix} &= \begin{bmatrix}0 \\ -(2m+m_b)g\end{bmatrix} + R(\theta_1)\begin{bmatrix}0 \\ T_1\end{bmatrix} + R(\theta_2)\begin{bmatrix}0 \\ T_2\end{bmatrix}.
\end{aligned} \tag{4.1}$$

Optimization variables

Through the equations of the movement of the system, 4 control inputs and 10 states are identified, that completely describe the dynamics of this system, and are the following

$$U = \begin{bmatrix} T_1 & T_2 & \tau_1 & \tau_2 \end{bmatrix}^T, \tag{4.2}$$

$$X = \begin{bmatrix} x_b & y_b & \theta_b & \theta_1 & \theta_2 & \dot{x}_b & \dot{z}_b & \dot{\theta}_b & \dot{\theta}_1 & \dot{\theta}_2 \end{bmatrix}^T. \tag{4.3}$$

Reference trajectory

In this problem, the center of mass of the system coincides with the center of mass of the bar. That is, the reference to the final position of the system is applied as a reference to the final position of the bar.

Thus, the setpoint vector for the states, X^*, takes into account the objective of the system to reach a given final position (x_b, z_b)=(x_b^*, z_b^*), without velocity. That is, with linear velocities equal to $\dot{x}_b = \dot{z}_b = 0$, as well as angular velocities equal to $\dot{\theta}_b = \dot{\theta}_1 = \dot{\theta}_2 = 0$. It is also wanted that the system finishes the trajectory in balance, maintaining an angle of $0°$.

Other objectives considered are that the vehicles reach the final position hovering. For this purpose, the total thrust force exerted on each vehicle must be equal to the force of gravity ($g = 10\ m/s^2$). It is also wanted that the forces generated by the rotors of each bi-rotor are of equal intensity. Thus, a null reference is applied to the pitching moments, τ_1 and τ_2. Note that, equating (3.10) to 0, it is proved that $F_1 = F_2$ and $F_3 = F_4$.

In summary, the setpoint vectors for X and U are as follows

$$\begin{aligned} X^* &= \begin{bmatrix} x_b^* & z_b^* & 0 & 0 & 0 & 0 & 0 & 0 & 0 & 0 & 0 & 0 & 0 & 0 \end{bmatrix}, \\ U^* &= \begin{bmatrix} 10 & 10 & 0 & 0 \end{bmatrix}. \end{aligned} \tag{4.4}$$

Cost function

The cost function must be formulated in such a way that its minimization defined in the optimization problem results in a satisfaction of the control objectives. In this example, the control objectives are system stabilization and trajectory optimization. The quadratic function is a widely used choice in optimal control problems and, in this example, it is a choice that is suitable because its minimization leads to an optimal global solution, under certain premises, such as considering an unconstrained linear system. This function is defined by quadratically weighing the distance between the states and the control inputs and the previously defined setpoint vectors.

For this problem, the cost function is then given by

$$J = \sum_{i=1}^{H} [(X(k+i) - X^*(k+i))^T Q (X(k+i) - X^*(k+i)) + (U(k+i) - U^*(k+i))^T R_Q (U(k+i) - U^*(k+i))], \tag{4.5}$$

where Q and R_Q correspond, respectively, to the weight factors that are applied to the states and to the control inputs.

Optimization problem

The optimization problem defined refers to a situation in which the maneuver is a diagonal trajectory. However, for the other type of maneuver that will be seen ahead, the reference to the final position is adjusted.

Adopting a model predictive control approach, at each iteration step k, a finite horizon optimization problem with horizon H is solved and the first element of the optimal control input is applied. Considering the desired trajectory X^* and the corresponding input U^*, the optimization problem for each iteration is now defined

$$\underset{U,X}{\text{minimize}} \qquad J$$

subject to

$$\begin{aligned}
\ddot{\theta}_1 &= \frac{\tau_1}{J_1}, \\
\ddot{\theta}_2 &= \frac{\tau_2}{J_2}, \\
\ddot{\theta}_b &= \frac{T_2 \cos(\theta_2 - \theta_b) - T_1 \cos(\theta_1 - \theta_b)}{J_b + m\frac{c^2}{2}}, \\
\ddot{x}_b &= \frac{-T_1 \sin\theta_1 - T_2 \sin\theta_2}{2m + m_b}, \\
\ddot{z}_b &= -g + \frac{T_1 \cos\theta_1 + T_2 \cos\theta_2}{2m + m_b}.
\end{aligned} \tag{4.6}$$

Simulation Results

This section presents different simulation of maneuvers for the system. In the following simulations, the bar is represented by an orange line segment. The maneuvers carried out were chosen in order to vary the trajectory that the system performs and understand if its movement remains continuous and smooth.

Maneuver 1 - Upward diagonal

In this example, the maneuver to be performed by the system is an ascending diagonal. As can be seen, the system completes the maneuver and reaches the reference for the final position $(x_b, z_b) = (5, 5)$. However, the system does not always move in a continuous smooth manner. In fact, this situation is evidenced by the curved appearance at the beginning of the system trajectory whose behavior only changes ahead, when the system starts to adopt a direct forward motion.

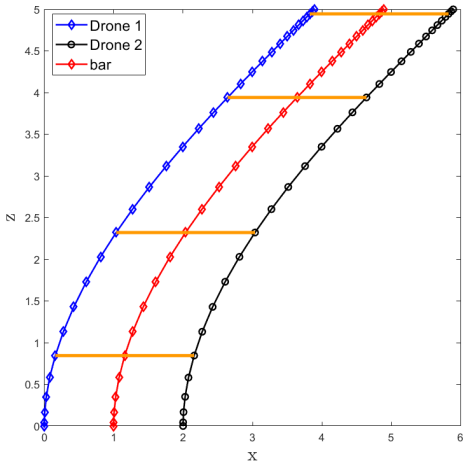

Figure 4.1: Upward diagonal maneuver for $H = 15$, $T_s = 0.2$.

Maneuver 2 - Sinusoidal Curve

The second maneuver to be performed is a half a period of a sinusoidal curve. The system reveals a rigid behavior when changing direction. As can be seen, the initial curve to the left is not accentuated, compared to the curve that occurs later, to the right. Although the trajectory reference is the half period of the sinusoidal curve, in fact the result that occurs cannot be considered a sinusoidal curve because the behavior of the system is not smooth as it happens in a sine wave.

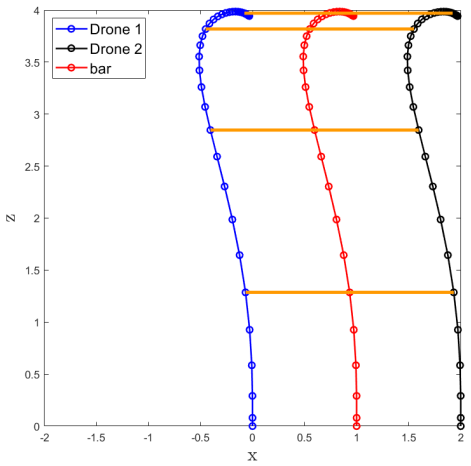

Figure 4.2: Sinusoidal Curve for $H = 10$, $T_s = 0.3$.

Maneuver 3 - Downward diagonal

The final maneuver to be performed is the descending diagonal. As in the case of an upward diagonal maneuver, the system assumes a non-smooth behavior at the beginning of the trajectory and roughly in the middle of the path, it starts to adopt a continuous smooth behavior by performing a direct diagonal trajectory.

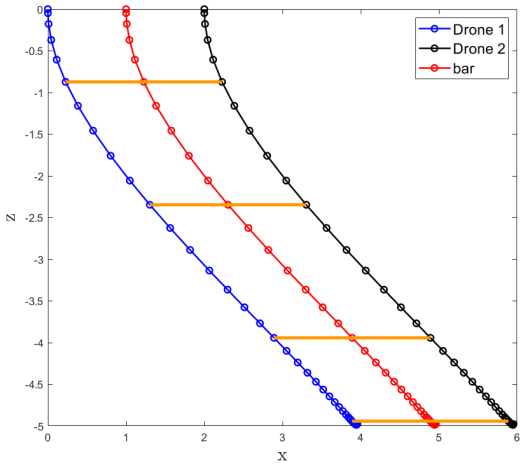

Figure 4.3: Downward diagonal for $H = 15$, $T_s = 0.2$.

Despite the system reaching the objectives of reference tracking, it was possible to conclude that it has a rigid behavior in the maneuvers performed. In order to make a more detailed analysis of the behavior of the controller developed for this system, in the next section an analysis of its performance is made.

Evaluation of system performance

In this section, the performance of the system is compared as a function of the following parameters: sampling time, T_s, and prediction horizon, H. The penalty for the control variables T_1 and T_2 is also considered. This penalization is carried out by varying a weight associated with these control inputs in the cost function, designated as weight β.

In order to evaluate the performance of the system, it is necessary to define evaluation measures. The first measure to be adopted is the cost, J, that quantifies the error between the values of the optimization variables and the defined setpoints. This value is presented in the form of a real number and, in most optimization problems, the goal is to minimize J.

Another measure considered is the root mean squared relative to the state vector, σ_X. σ_X evaluates the deviation between the state vector, X_i, and the setpoint vector, $\hat{X}_i$, and is given by

$$\sigma_X = \sqrt{\frac{1}{N}\sum_{i=1}^{N} \|X_i - \hat{X}_i\|^2}, \tag{4.7}$$

where N is the total number of samples.

Finally, root mean square of the control vector, σ_U, is considered, which refers to the magnitude of the control vector. σ_U is given by

$$\sigma_U = \sqrt{\frac{1}{N}\sum_{i=1}^{N} \|U_i\|^2}, \tag{4.8}$$

where U corresponds to the control vector.

It can now be concluded that the purpose of this section is to find the values for which the returned values of J and σ_X are minimal and also evaluate the value of σ_U for each situation.

Prediction Horizon H

Figures 4.4 and 4.5 show the evolution of the system for different values of the prediction horizon, H, and for $T_s = 0.2$, evaluated through the measures mentioned above.

By observing the simulation of J as a function of H and the values of J for the different values of H shown in Table 4.1, it is concluded that the minimum value of the cost function,is reached for $H = 20$. From $H = 20$, J takes higher values, which is undesirable.

Since these simulations are carried out in a limited time interval, the output variance is finite and it is thus possible to ascertain the value of H from which the system stabilizes. By analyzing the simulation of σ_X as a function of H and also the values presented in Table 4.1, it is possible to conclude that the system stabilizes from $H = 15$. In conclusion, in order for the system control to be satisfactory, for simulations whose sampling time is $T_s = 0.2$, a stabilizing value of H must be used, ($H \geqslant 15$), considering that any H between $H = 15$ and $H = 20$ results in minimum values for J.

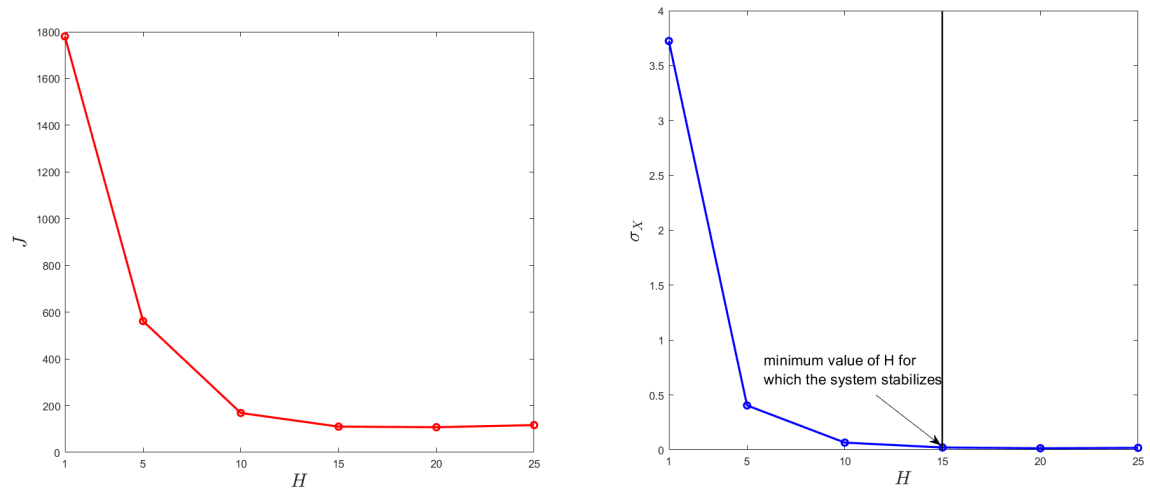

(a) J (b) σ_X

Figure 4.4: Evolution of system performance through measures J and σ_X for different H and $T_s = 0.2$.

The root mean square of the control, σ_U, allows measurements to be made in relation to the power spent in controlling the system. By observing Figure (4.5), it can be concluded that the minimum value of σ_U occurs for $H = 20$, which is a stabilizing prediction horizon value of the system and whose value corresponds to a minimum value of J. It makes sense that the minimum value of σ_U occurs for $H = 20$ since the control objectives are represented in the cost function and, when J is minimum, all predefined requirements are met. In addition, a stabilized system will use less power than an unstable system.

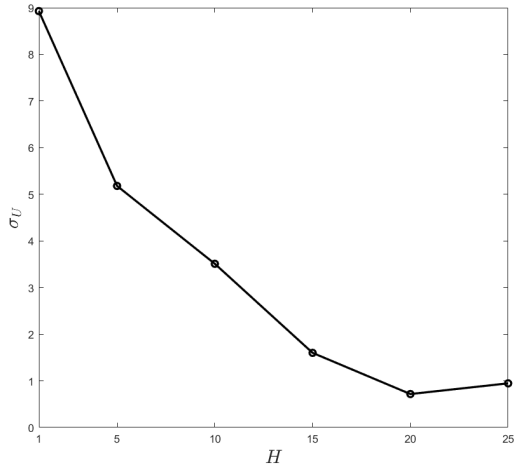

Figure 4.5: Evolution of system performance through σ_U for different H for $T_s = 0.2$.

Table 4.1 shows the values of J and σ_X for different values of H, thus summarizing the conclusions drawn above.

	$H = 5$	$H = 10$	$H = 15$	$H = 20$	$H = 25$
J	561.9	168.5	110.2	107.6	116.8
σ_X	0.45	0.067	0.02	0.015	0.018

Table 4.1: Comparison of the values of J and σ_X for different values of H.

Sampling time T_s

The performance of the system is now evaluated for different values of the sampling time, T_s and for $H = 15$. In Figure 4.6, the simulations for J and σ_X as a function of the sampling time, Ts, are shown. Through the analysis of the simulation of J, it is concluded that the cost function reaches a minimum value for $T_s = 0.3$, taking from there always higher values. Note that the desirable value of J is always the minimum value as it is when J is minimum, the difference between the optimization variables and the desired reference trajectory is also minimal. In addition, in this situation, other control objectives considered in the function are achieved.

In this example it is also possible to ascertain the value of H from which the system stabilizes since the simulations are carried out within a limited time interval, which results in a finite output variance. From the observation of σ_X simulation, it is concluded that the system stabilizes from $T_s = 0.2$ up to $T_s = 0.4$. From $T_s = 0.4$, the error evaluated between the state vector, Y_i, and the setpoint vector, $\hat{X}_i$, increases significantly, which compromises the stability of the system.

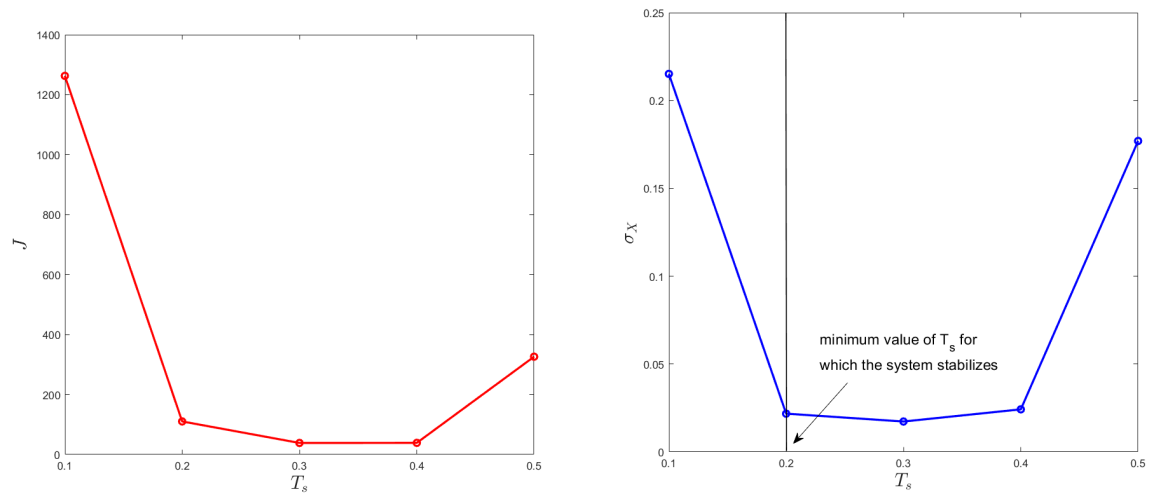

(a) J (b) σ_X

Figure 4.6: Evolution of system performance through measures J and σ_X for different T_s and $H = 15$.

Fig. 4.7 shows the simulation of σ_U as a function of T_s. Once again, the minimum value of σ_U coincides with the minimum value of J, which is coherent, since a minimum value of J implies less power expenditure. Additionally, the minimum value of σ_U also coincides with the minimum value of σ_X, which is also consistent since a stable system should use very little power.

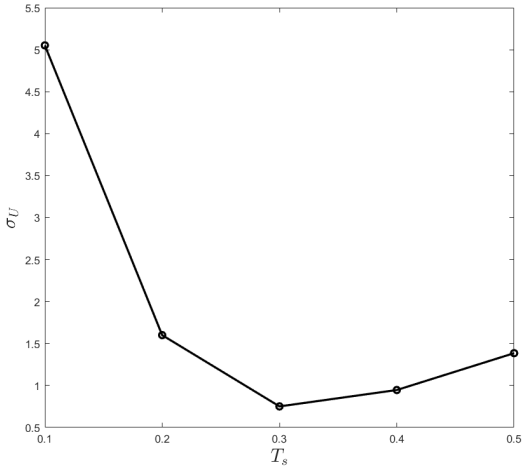

Figure 4.7: Evolution of system performance through measure σ_U for different T_s and for $H = 15$.

In short, to achieve the final objective of satisfactorily controlling the system, a value of T_s between $T_s = 0.2$ and $Ts = 0.4$ should be chosen for simulations for $H = 15$. Ideally, a value of $T_s = 0.3$ should be chosen in order to consider a minimum value of J for the optimization problem considered.

Table 4.2 shows the values of J and σ_X for different values of T_s, which corroborate the conclusions drawn above.

	$T_s = 0.1$	$T_s = 0.2$	$T_s = 0.3$	$T_s = 0.4$	$T_s = 0.5$
J	1263	110.2	38.44	38.75	326.2
σ_X	0.2152	0.02	0.017	0.024	0.18

Table 4.2: Comparison of the values of J and σ_X for different values of T_s.

It can now be concluded that the diagonal maneuvers (ascending and descending) carried out in the previous section would have had a more satisfactory result in terms of cost if the chosen value for T_s was $T_s = 0.3$. However, the stability of the system would not improve significantly. For the second maneuver, it is not possible to draw such conclusions as the prediction horizon value considered is different from the one considered in this example.

Penalization of the control variables T_1 and T_2: weight β

Figures 4.8 and 4.9 show the performance of the system for different values of weight β, which is a variable penalty for the control variables T_1 and T_2. The increase in β means that less value is given to these control inputs, compared to other optimization variables present in the cost function, which can compromise the control of the system depending on the magnitude of the penalty applied.

Through the analysis of the simulation of J as a function of β, it can be concluded that the minimum value of J is reached for $\beta = 1$. This conclusion is coherent since, in a situation where $\beta = 0$, the total thrust forces exerted on each drone are not considered, which is not representative of the system. That is, not considering half of the system control variables, naturally leads to a higher cost. On the other hand, in situations where $\beta > 1$, T_1 and T_2 are considered to be of little importance compared to other optimization variables present in the cost function.

In this example, it is also possible to ascertain the value of H from which the system stabilizes. Observing the simulation of β in function of H, it is concluded that although σ_X takes practically the same value for $\beta = 0$ and for $\beta = 1$, the first case describes a situation in which the control variables T_1 and T_2 are not included in the cost function, which is not representative of the system. In addition, this situation occurs because T_1 and T_2 tend towards a value close to 0 and, therefore, their exclusion from the function does not have a significant numerical value. However, it negatively impacts the stability of the system and results in a high J.

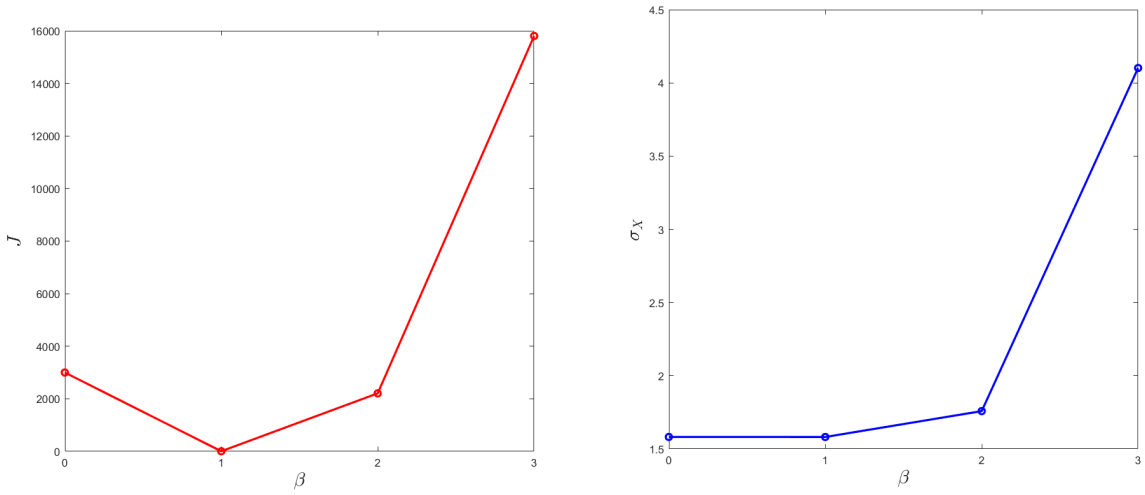

(a) J (b) σ_X

Figure 4.8: Evolution of system performance through measures J and σ_X for different β and for $H = 15$ and $T_s = 0.2$.

Fig. 4.9 shows the simulation of σ_U as a function of H. In this case, the minimum value of σ_U coincides with a situation where $\beta = 2$. In this situation, the amplitude of these control variables is smaller and therefore there is less power consumption. From $\beta = 2$ on, J and σ_X increase, as well as the power consumption, which is reflected by a higher value of σ_U.

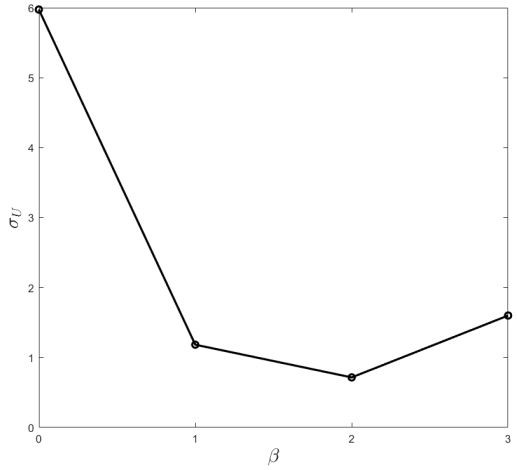

Figure 4.9: Evolution of system performance through measure σ_U for different β and for $H = 15$ and $T_s = 0.2$

Chapter 5

Control of the quadcopters bar system

This chapter addresses the control of two drones that cooperate with the objective of transporting a bar, which is an object that requires to be transported by more than one vehicle. In this chapter, the control problem is defined and simulations are presented in order assess the control strategy adopted for this system.

System dynamics

The dynamics obtained for this system, previously defined in chapter 3, are given by

$$\begin{aligned} \ddot{p}_b^I &= -ge_3 + \frac{T_O}{m_{sys}}, \\ I\dot{w}^{B_1} &= -w^{B_1} \times Iw^{B_1} + \tau^{B_1}, \\ I\dot{w}^{B_2} &= -w^{B_2} \times Iw^{B_2} + \tau^{B_2}, \\ I_{sys}\dot{w}^O &= -w^O \times I_{sys}w^O + \tau^O. \end{aligned} \tag{5.1}$$

Optimization variables

From the equations of system movement defined in (5.1), 20 states and 8 control inputs are identified, given by

$$\begin{aligned} U &= \begin{bmatrix} T_1 & \tau_{x1} & \tau_{y1} & \tau_{z1} & T_2 & \tau_{x2} & \tau_{y2} & \tau_{z2} \end{bmatrix}^T, \\ X_1 &= \begin{bmatrix} \phi_1 & \theta_1 & \psi_1 & w_{x1} & w_{y1} & w_{z1} \end{bmatrix}^T, \\ X_2 &= \begin{bmatrix} \phi_2 & \theta_2 & \psi_2 & w_{x2} & w_{y2} & w_{z2} \end{bmatrix}^T, \\ X_b &= \begin{bmatrix} x_b & y_b & z_b & \dot{x}_b & \dot{y}_b & \dot{z}_b & \psi_b & w_{z_b} \end{bmatrix}^T, \\ X &= \begin{bmatrix} X_1 & X_2 & X_b \end{bmatrix}^T. \end{aligned} \tag{5.2}$$

Reference trajectory

In this problem, the center of mass of the system coincides with the center of mass of the bar. Thus, the reference for the final position of the system is applied to the position of the bar, whose final desired position is $(x_b, y_b, z_b) = (x_b^*, y_b^*, 0)$. Note that it is considered a null reference for z_b since the system moves only in the xy-plane, when $z = 0$.

Regarding the references applied to the remaining states, it is wanted that the system ends the trajectory with zero linear and angular velocities. Additionally, it is desired that each of the three bodies assume an angle of $0°$, keeping the system in balance when the final position is reached.

Another of the considered objectives is that the vehicles reach the final position hovering. Therefore, the total force exerted on each vehicle must be equal to the force of gravity ($g = 10\ m/s^2$). Additionally, a null reference is considered for the pitching moments generated by the rotors of each drone, in order to consider that each force generated by the rotors (F_1, F_2, F_3 and F_4) is of equal intensity (Equating (3.28) to 0 results in $F_1 = F_2 = F_3 = F_4$).

In summary, the setpoint vectors for X and U are as follows

$$\begin{aligned} X^* &= \begin{bmatrix} 0 & 0 & 0 & 0 & 0 & 0 & 0 & 0 & 0 & 0 & 0 & 0 & x_b^* & y_b^* & 0 & 0 & 0 & 0 & 0 & 0 \end{bmatrix}, \\ U^* &= \begin{bmatrix} 10 & 0 & 0 & 0 & 10 & 0 & 0 & 0 \end{bmatrix}. \end{aligned} \tag{5.3}$$

Cost function

The cost function must be a mathematical representation of the control objectives. In this example, the control objectives are system stabilization and trajectory optimization. Thus, it was considered appropriate to use a quadratic function for the cost function, where the deviation from the desired setpoints is measured. In this problem, the cost functions are given by

$$J = \sum_{i=1}^{H} [(X(k+i) - X^*(k+i))^T Q (X(k+i) - X^*(k+i)) + (U(k+i) - U^*(k+i))^T R_Q (U(k+i) - U^*(k+i))]. \tag{5.4}$$

where Q and R_Q correspond, respectively, to the weight factors that are applied to the states and to the control inputs associated with both drones.

Optimization problem

The optimization problem defined takes into account a situation in which the maneuver to be carried out is simple: a rectilinear trajectory. For the other type of maneuver that will be seen ahead, the reference value for the final position $(x_b, y_b, 0)$, present in the vector X^*, is adjusted.

Adopting a model predictive control approach, at each iteration step k, a finite horizon optimization problem with horizon H is solved and the first element of the optimal control input is applied. Considering the desired trajectory X^* and the corresponding input U^*, the optimization problem for each iteration is

now defined

$$\underset{U_1,U_2,X_1,X_2,X_b}{\text{minimize}} \quad J$$

subject to

$$\begin{aligned} \ddot{p}_b^I &= -ge_3 + \frac{T_O}{m_{sys}}, \\ I_1\dot{w}^{B_1} &= -w^{B_1} \times I_1 w^{B_1} + \tau^{B1}, \\ I_2\dot{w}^{B_2} &= -w^{B_2} \times I_2 w^{B_2} + \tau^{B_2}, \\ I_{sys}\dot{w}^O &= -w^O \times I_{sys} w^O + \tau^O. \end{aligned} \tag{5.5}$$

Simulation Results

Note that the positions of the two quadcopters, p_{D1}^I and p_{D2}^I seen in the XY frame, can be defined through the bar generalized coordinates, x_b, y_b and ψ_b, as follows

$$\begin{aligned} x_1 &= x_b - \frac{c}{2}\cos(\psi_b), \\ x_2 &= x_b + \frac{c}{2}\cos(\psi_b), \\ y_1 &= y_b - \frac{c}{2}\sin(\psi_b), \\ y_2 &= y_b + \frac{c}{2}\sin(\psi_b). \end{aligned} \tag{5.6}$$

Thus, it is possible to represent not only the trajectory of the bar, but also the trajectories of both vehicles. The figures below show the simulations corresponding to three different trajectories, where the bar is represented by an orange line segment.

Maneuver 1 - Rectilinear trajectory

In this example, the final position is $(x_b, y_b) = (0.5, 5)$ and therefore the movement to be carried out is a straight upward movement. This is a simple movement and for this reason it was successfully executed by the system, whose trajectory is as direct as possible.

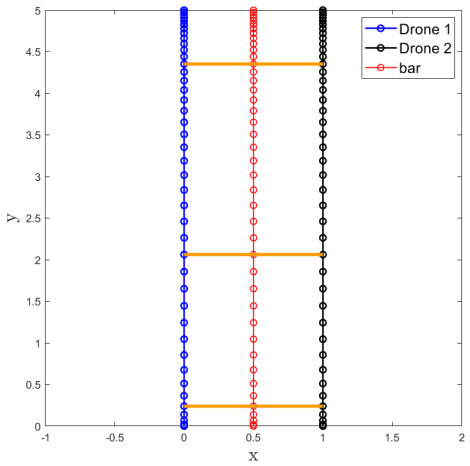

Figure 5.1: Rectilinear trajectory for $H = 7, Ts = 0.2$.

Maneuver 2 - Circular path

In the examples from Figure 5.2 to Figure 5.4, a circular reference trajectory is considered, for different initial conditions. It is noticeable that in the first example the system successfully follows the defined reference. However, in the examples that follow, where the initial condition of the system takes a value that is located inside or outside the circle, the system initially does not follow the reference closely and takes time until it starts to draw a circular path.

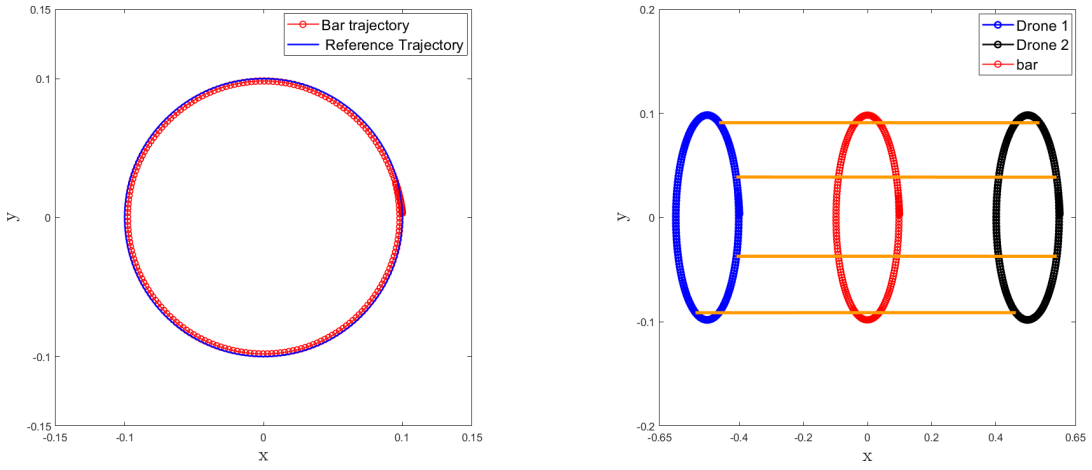

(a) Bar trajectory

(b) System trajectory

Figure 5.2: Circular path for $H = 12$,$T_s = 0.2$ and $x(0) = \begin{bmatrix} 0.1\cos(0.01\pi) & 0.1\sin(0.01\pi) & 0 \end{bmatrix}^T$.

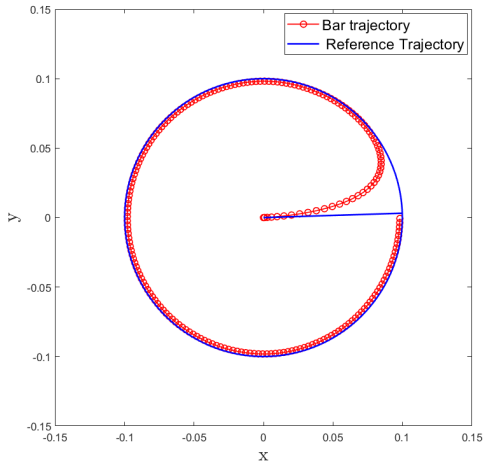

(a) Bar trajectory

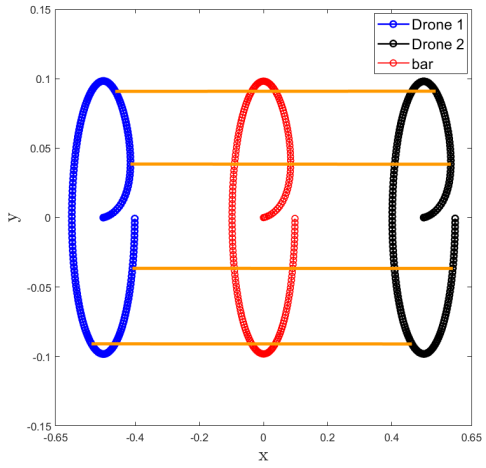

(b) System trajectory

Figure 5.3: System Trajectory for $H = 12, T_s = 0.2$ and $x(0) = \begin{bmatrix} 0 & 0 & 0 \end{bmatrix}^T$.

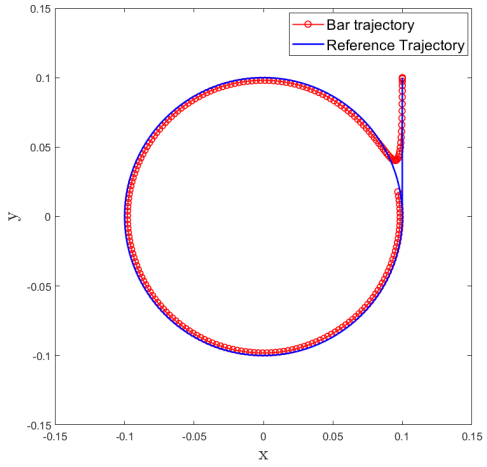

(a) Bar trajectory

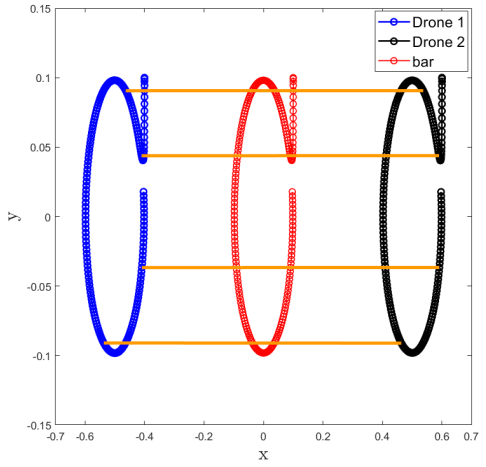

(b) System trajectory

Figure 5.4: System Trajectory for $H = 12, T_s = 0.2$ and $x(0) = \begin{bmatrix} 0.1 & 0.1 & 0 \end{bmatrix}^T$.

Chapter 6

Drone replacement strategy

The benefit of addressing the problem of the drone autonomy is that the transport task performed through the cooperation of vehicles does not have to be interrupted if one of the drones has reached its maximum energy consumption and is unable to continue. Thus, if necessary, the replacement of drones can occur during the mission and the task can be carried out continuously until the end. Note that the solution to this problem takes into account the replacement of UAVs and not batteries, since the latter situation would force the multi-drone system to stop.

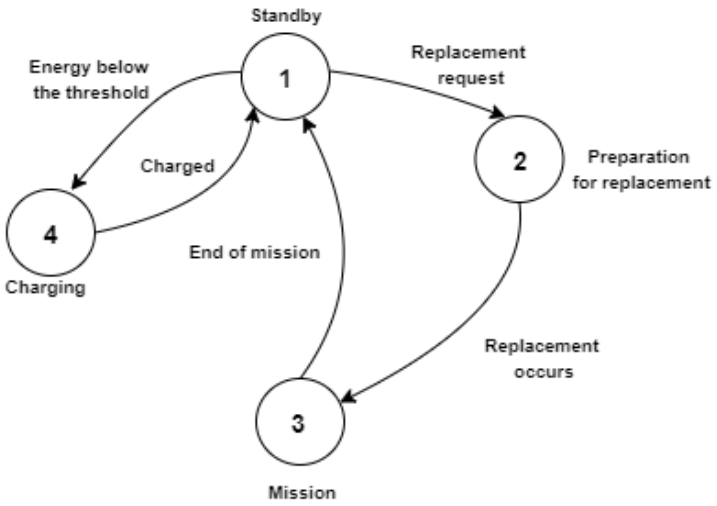

Figure 6.1: Drone state machine during a mission (Adapted from [9]).

The diagram shown in Fig. 6.1, depicts a situation in which a UAV intervenes in the transport mission in order to replace one of its peers who does not have enough autonomy to continue the task. In this context, consider an initial situation in which the drone that is waiting to intervene is at a base station with its battery fully charged.

It is assumed that the drones participating in the transport mission are replaced one at a time. That is, of the drones that carry out the mission, there are never two or more vehicles that enter a low energy state at the same time. Additionally, while the replacement vehicle is charging, it is assumed that all

drones that are carrying out the assigned task, have autonomy to continue the mission.

The replacement drone goes through the following states

1. **Standby** - The replacement drone is waiting for a replacement request to appear, with its battery charged, at the base station.
2. **Preparation for replacement** - It is assumed that the drone that is waiting to intervene, automatically enters this state when the energy threshold of any of the drones participating in the mission is reached. The drone that will do the replacement is ready to position itself. Therefore, it approaches the formation assuming the position of the vehicle to be replaced.
3. **Mission** - At this state, the mission is being carried out. The replacement drone took the position of the drone to be replaced and the drone to be replaced has returned to the base station.
4. **Charging** - In this state, the replacement vehicle is charging at the station.

Energy consumption model

In order to optimize the vehicle replacement process, it is necessary to efficiently manage the energy of each vehicle. For that purpose, this section addresses the problem of minimizing energy consumption of drones.

The energy model resembles an integrator since the battery of each drone is charged at the charging stations and discharged when the vehicle is in motion. Table 6.1 shows the values of the parameters used in the simulations present in this section.

	Symbol	Value
Mass of drone body [kg]	m_1,m_2	1
Mass of bar [kg]	m_{bar}	0.5
Drone battery energy [J/kg] [10]	E_0	5.4

Table 6.1: Adapted parameters for drone replacement problem.

The problem of minimizing the energy consumption of each vehicle introduces a state E_{C_i} for each vehicle i ($i = 1, 2$), which represents the energy consumed by each drone per unit of time. Thus, the derivative of E_{C_i}, $\dot{E}_{C_i}$, represents the energy consumption rate of each drone per unit of time.

The power corresponds to the rate of the work that is performed, whose formula is proportional to the force times the speed. Therefore, by analogy, $\dot{E}_{c_i}$ is given by

$$\dot{E}_{C_i} = K_i \left| v_i^T \dot{v}_i \right| + \left| w_i^T I_i \dot{w}_i \right|, \quad i = 1, 2, \tag{6.1}$$

where $K_i = m_i + m_{bar}\gamma$, $(i = 1, 2)$ is a coefficient that describes the impact of the weight of the vehicle and the weight of the bar on the energy consumption rate of the drone. In this coefficient, a binary decision variable γ was adopted. This variable has two possible states: if $\gamma = 1$, the drone in question is carrying the bar and if $\gamma = 0$, the bar is not being transported. Based on the value of the parameters defined above, it is concluded that the weight of the bar adds a 50% energy expense to the energy consumption rate of each vehicle, since $K_i = 1.5$, when $\gamma = 1$.

Additionally, I_i corresponds to the inertial matrix of each drone i ($i = 1, 2$). The inertial matrix for drone 1 is given by

$$I_1 = \begin{bmatrix} I_{xx_{sys}} & 0 & 0 \\ 0 & I_{yy_{sys}} & 0 \\ 0 & 0 & I_{zz_{sys}} \end{bmatrix},$$

where each non-null entry of the matrix corresponds to the moment of inertia of the system constituted by the drone and the bar, in each direction (x, y and z). On the other hand, I_2 has two distinct values, depending on the instant of time where the dynamics of drone 2 acts. From $k = t_1$ to $k = t_2$, I_2 is given

by

$$I_2 = \begin{bmatrix} I_{xx} & 0 & 0 \\ 0 & I_{yy} & 0 \\ 0 & 0 & I_{zz} \end{bmatrix},$$

that is, it only takes into account the moments of inertia related to the drone, since in this period of time the bar is not being transported. From $k = t_2$ to $k = t_f$, $I_2 = I_1$, since drone 2 is transporting the bar in that time interval.

It is also important to note that the energy available for each drone per unit of time, E_{D_i}, is given by

$$E_{D_i} = E_0 - E_{C_i}, \tag{6.2}$$

where E_0 corresponds to the battery energy for each drone.

Suboptimal solution to the optimal state transfer problem

In order to address the problem of vehicle energy consumption, the following situation is analyzed. Consider a drone (drone 1) that departs from the base station located at $(x, y) = (0, 0)$, carrying a bar. It is assumed that this vehicle does not have enough energy available to reach a predefined final position. Thus, the intervention of another vehicle is necessary. More precisely, drone 2 departs from the same station and meets his peer, at a given moment. From that moment, drone 2 will transport the bar, until the end of the predefined trajectory.

In this context, it is also assumed that

- Each drone is able to transport the bar.
- For the sake of simplicity, it is considered that the bar is a mass point and that the battery energy value for each drone is $E_0 = 5.4\ J$ (previously defined in Table 6.1.
- Drone 2 will depart from the base at a moment when drone 1 has low battery (less than 30%), that is, in the time interval where $E_{D_1} =]0, 0.3E_0]$.
- In this scenario, charging stations are not considered.

Regarding the replacement of drone 1, a question arises: **What will be the optimum moment, t_1, when drone 2 should depart from the base in order to assist drone 1, with the objective of minimizing the energy consumption of both vehicles?** The purpose of this section is to find the answer to this question.

System under analysis

The system under analysis incorporates two continuous dynamic systems that correspond to dynamics of each vehicle. In addition to the control variables associated with the model of each drone, an independent decision control variable is considered: the switching time, t_1.

In this problem, the system is divided as follows

- Subsystem 1, which is active in the interval $\left[t_0, \quad t_1\right]$:

$$\dot{x_1} = f_1(x_1, u_1), \; t_0 \leq t \leq t_1, \tag{6.3}$$

where $t_0 = 1$, in discrete time.

- Subsystem 2, which is active in the interval $\left[t_1 + 1, \quad t_f\right]$:

$$\dot{x_2} = f(x_2, u_2), \; t_1 + 1 \leq t \leq t_f. \tag{6.4}$$

In Figure 6.2, the problem under analysis is represented. The trajectory of the system starts at a given initial state, x_0, and progresses to a final state, x_f. The state X_1 marks the transition between the first and the second set of dynamics. The problem then lies in deciding the optimal instant time, t_1, where the switch should be made.

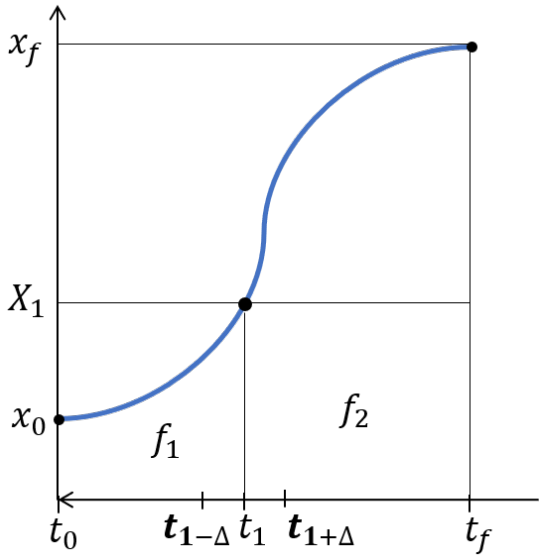

Figure 6.2: Explanation of the energy consumption optimization problem.

Interval Search

In order to solve the drone autonomy problem, an algorithm is proposed, that calculates t_1 through a search made by intervals, based on the minimum cost associated with each instant of time. For this purpose, an initial estimate is defined, $\hat{t_1}$, contained in the candidate values for t_1. The pseudo-code for the algorithm is shown below.

Algorithm 1: Interval Search algorithm

Result: t_1 value.

```
/* Run trajectory optimization simulation once and set initial time range:  */
```

Initialization

Set start interval $t = \left[\hat{t_1} - \Delta \quad \hat{t_1} \quad \hat{t_1} + \Delta\right]$.

for ($k = t_0 : 1 : t_f$ **)** {

- `// Calculate cost for each element of interval` t
- J= cost
- **if** *minimum*(J) *and* $k > t_0$ *and* k*= far left of* t **then**
  - `// If the minimum value of` J `is at the far left of` t`, the procedure is repeated with the interval shifted one unit to the left.`
  - Perform a left shift by Δ and repeat the algorithm.
- **end**
- **if** *minimum*(J) *and* $k < t_f$ *and* k*=far right of* t **then**
  - `// If the minimum value of` J `is at the far right of` t`, the procedure is repeated with the interval shifted one unit to the right.`
  - Perform a right shift by Δ and repeat the algorithm.
- **end**
- **if** *minimum*(J) *and* k*= central value of* t **then**
  - `// If the minimum value of` J `is in the middle element of` t`, then the optimal value,` t_1`, corresponds to that value of` t`.`
  - $t_1 = k$.
- **end**
- **if** *minimum*(J) *and* $k = t_0$ *and* k*= far left of* t *or minimum*(J) *and* $k = t_f$ *and* k*= far right of* t **then**
  - `// If the minimum value of` J `is in the left element of` t`, which corresponds to the first instant of the simulation, then the optimal value` t_1 `corresponds to that value of` t `or if the minimum value of` J `is in the right element of` t`, which corresponds to the last instant of the simulation, then the optimal value,` t_1`, corresponds to that value of` t`.`
  - $t_1 = k$.
- **end**

}

Note that this is a sub-optimal solution since the candidate values for t_1 are multiples of the sampling time, $T_s = 0.1$, there being other possible values that are not considered in this problem.

Problem Formulation

In this example, two different scenarios are considered for transporting the bar.

- **Case 1** - It is considered that both vehicles are symmetrical. That is, the two drones have the same mass and the same geometry.
- **Case 2** - In this case, drone 1 follows the description of the vehicles considered in case 1, while drone 2 presents a difference in geometry which causes that, when transporting the bar, it consumes more energy than the first drone. The value considered for the mass of the bar that this vehicle transports is now $m_{bar} = 0.9\ kg$. Thus, when drone 2 transports the bar, there is an additional energy expense of 90% to its energy consumption rate, instead of the 50% expenditure considered in the previous case.

  For both problems there are three variants of the energy consumption model, depending on what time the system is operating.

  – From $k = 1$ to $k = t_1$, the dynamics of drone 1 are active, with the following energy consumption model

  $$\dot{E}_{C_1} = K_1 \left| v_1^T \dot{v}_1 \right| + \left| w_1^T I_1 \dot{w}_1 \right|, \tag{6.5}$$

  where $K_1 = m_1 + m_{bar}$.

  – From $k = t_1 + 1$ to $k = t_f$, the dynamics of drone 2 are active, and its energy consumption model varies depending on the time interval in which dynamics 2 are acting. Its energy consumption model is given by

  $$\dot{E}_{C_2} = K_2 \left| v_2^T \dot{v}_2 \right| + \left| w_2^T I_2 \dot{w}_2 \right|, \tag{6.6}$$

  where

  $$\begin{cases} K_2 = m_2, & k = t_1 + 1, \cdots, t_2 - 1. \\ K_2 = m_2 + m_{bar}, & k = t_2, \cdots, t_f. \end{cases}$$

System control

System dynamics

For this example, the dynamics of each vehicle are active at different times, whose equations of motion are defined in chapter 3. Note that the dynamics of the system is composed of the dynamics of each drone and also the respective model of energy consumption defined in (6.5) and (6.6). That is, from $k = 1$ to $k = t_1$, the following dynamics are active

$$\begin{aligned} I\dot{w}^{B_1} &= -w^{B_1} \times Iw^{B_1} + \tau^{B_1}, \\ (m_1 + m_{bar})\ddot{p}_1 &= -(m_1 + m_{bar})ge_3 + T_1 R^I_{B_1} e_3, \\ \dot{E}_{C_1} &= K_1 \left| v_1^T \dot{v}_1 \right| + \left| w_1^T I_1 \dot{w}_1 \right|, \end{aligned} \tag{6.7}$$

and from $k = t_1 + 1$ to $k = t_f$ the active dynamics are given by

$$\begin{aligned} I\dot{w}^{B_2} &= -w^{B_2} \times Iw^{B_2} + \tau^{B_2}, \\ (m_2 + m_{bar}\gamma)\ddot{p}_2 &= -(m_2 + m_{bar}\gamma)ge_3 + T_2 R^I_{B2} e_3, \\ \dot{E}_{C_2} &= K_2 \left| v_2^T \dot{v}_2 \right| + \left| w_2^T I_2 \dot{w}_2 \right|. \end{aligned} \tag{6.8}$$

Optimization variables

From the equations of system movement defined in (6.7) and (6.8), 26 states and 8 control inputs are identified, given by

$$\begin{aligned} U_1 &= \begin{bmatrix} T_1 & \tau_{x1} & \tau_{y1} & \tau_{z1} \end{bmatrix}^T, \\ U_2 &= \begin{bmatrix} T_2 & \tau_{x2} & \tau_{y2} & \tau_{z2} \end{bmatrix}^T, \\ X_1 &= \begin{bmatrix} x_1 & y_1 & z_1 & \dot{x}_1 & \dot{y}_1 & \dot{z}_1 & \phi_1 & \theta_1 & \psi_1 & w_{x1} & w_{y1} & w_{z1} & E_{C_1} \end{bmatrix}^T, \\ X_2 &= \begin{bmatrix} x_2 & y_2 & z_2 & \dot{x}_2 & \dot{y}_2 & \dot{z}_2 & \phi_2 & \theta_2 & \psi_2 & w_{x2} & w_{y2} & w_{z2} & E_{C_2} \end{bmatrix}^T. \end{aligned} \tag{6.9}$$

The setpoint vectors for X_1, X_2, U_1 and U_2 are defined taking into account the objectives referred to in (5.3), are given by

$$\begin{aligned} X_i^* &= \begin{bmatrix} x_i^*(k) & y_i^*(k) & 0 & 0 & 0 & 0 & 0 & 0 & 0 & 0 & 0 & 0 & 0 \end{bmatrix}, \\ U_i^* &= \begin{bmatrix} 10 & 0 & 0 & 0 \end{bmatrix}, \quad i = 1, 2. \end{aligned} \tag{6.10}$$

Cost function

In this example, the cost functions represent different control objectives, and are the following

- J_1 and J_2 are the costs associated with the movement of drone 1 and drone 2, respectively. These functions take into account the objectives of system stabilization and trajectory optimization. J_1 is defined from the instants $k \in 1, \ldots, t_1$ and J_2 is computed from the instant immediately after the switching instant, t_1, until the final simulation instant, t_f. Both functions are defined in eq.(5.4).

- J_{opt_1} and J_{opt_2} are the costs associated with minimizing the energy consumption of each drone that express the objective of finding an optimal flight speed in order to maximize the distance traveled by each vehicle. That is, it expresses the objective of minimizing the energy consumption of each drone. J_{opt_1} is calculated in the same time interval as J_1 as J_2 and J_{opt_2} are calculated in the same period of time.

The cost function must be formulated in such a way that its minimization defined in the optimization problem, results in a satisfaction of the control objectives. The quadratic function is a widely used choice in optimal control problems and, in this example, it is a choice that is suitable for the costs associated with the movement of drones, J_1 and J_2, since its minimization leads to an optimal global solution, under certain premises, such as considering an unconstrained linear system. Since J_{opt_1} and J_{opt_2} have different control objectives than J_1 and J_2, it is considered appropriate to use the module in the definition of these cost functions, in order to minimize the energy consumption of each vehicle per unit of time. This is also a usual choice for energy consumption minimization but other options could have could been made, taking into account convex functions of X_1, X_2, U_1 and U_2, as long as its definition was in line with the control objectives required by J_{opt_1} and J_{opt_2}. The cost functions considered in this problem are then given by

$$
\begin{aligned}
J_1 &= \sum_{i=1}^{H} [(X_1(k+i) - X_1^*(k+i))^T Q (X_1(k+i) - X_1^*(k+i)) + (U_1(k+i) - U_1^*(k+i))^T R_Q (U_1(k+i) - U_1^*(k+i))], \\
J_2 &= \sum_{i=1}^{H} [(X_2(k+i) - X_2^*(k+i))^T Q (X_2(k+i) - X_2^*(k+i)) + (U_2(k+i) - U_2^*(k+i))^T R_Q (U_2(k+i) - U_2^*(k+i))], \\
J_{opt_1} &= \sum_{i=1}^{H} [E_{C_1}(k+i) - \Gamma(\|v_1(k+i)\|^2)], \\
J_{opt_2} &= \sum_{i=1}^{H} [E_{C_2}(k+i) - \Gamma(\|v_2(k+i)\|^2)],
\end{aligned}
\tag{6.11}
$$

where Γ is a coefficient that when $\Gamma > 1$, attaches more importance to minimizing the energy consumption of the respective drone and when $\Gamma < 1$, it gives more importance to optimizing the velocity at which the vehicle moves. Additionally, Q and R_Q correspond, respectively, to the weight factors that are applied to the states and to the control inputs of both vehicles.

Problem constraints

In addition to the limitation of the battery of each vehicle as it is finite, another restriction regarding the transport of the bar is considered. An instant t_2 is defined, after t_1, where the second vehicle meets the first one so that, from then on, the bar can be transported by drone 2. Assuming that this instant is fixed, the new constraint determines that this moment will occur at $t_2 = t_1 + 0.3$ seconds.

Optimization problem

The optimization problem consists of minimizing the cost, subject to the system dynamics equations and the restrictions to the problem. Note that, in this example, the optimization variables correspond not only to the states and control variables of each drone but also to the optimal switching time, t_1. The optimization problem for this example is given by

$$\underset{U_1,U_2,X_1,X_2,t_1}{\text{minimize}} \quad J_{1_{k\in 1,\dots,t_1}} + J_{opt_{1\,k\in 1,\dots,t_1}} + J_{2_{k\in t_1+1,\dots,t_f}} + J_{opt_{2\,k\in t_1+1,\dots,t_f}}$$

subject to

$$\begin{aligned}
&for \;\; k = 1, \cdots, t_1 \\
&\quad I\dot{w}^{B_1} = -w^{B_1} \times Iw^{B_1} + \tau^{B_1}, \\
&\quad (m_1 + m_{bar})\ddot{p}_1 = -(m_1 + m_{bar})ge_3 + T_1 R^I_{B_1} e_3, \\
&\quad 0 < E_1 < E_0, \\
&\quad \dot{E}_{C_1} = K_1 \left| v_1^T \dot{v}_1 \right| + \left| w_1^T I_1 \dot{w}_1 \right|,
\end{aligned} \tag{6.12}$$

$$\begin{aligned}
&for \;\; k = t_1 + 1, \cdots t_f \\
&\quad I\dot{w}^{B_2} = -w^{B_2} \times Iw^{B_2} + \tau^{B_2}, \\
&\quad (m_2 + m_{bar}\gamma)\ddot{p}_2 = -(m_2 + m_{bar}\gamma)ge_3 + T_2 R^I_{B2} e_3, \\
&\quad 0 < E_2 < E_0, \\
&\quad \dot{E}_{C_2} = K_2 \left| v_2^T \dot{v}_2 \right| + \left| w_2^T I_2 \dot{w}_2 \right|,
\end{aligned}$$

$$p_1(t_2) = p_2(t_2),$$

where

$$\begin{cases} \gamma = 0, & k = t_1, \cdots, t_2 - 1. \\ \gamma = 1, & k = t_2, \cdots, t_f. \end{cases}$$

Choice of t_1

As mentioned before, the candidate values of t_1 are chosen in a time interval when the energy available of drone 1 per unit of time, E_{D_1}, is less than or equal to 30$\%$ of its initial energy, E_0.

Fig. 6.3 shows the candidate values for t_1 that are present in this interval (Δt), defined from $t_1 = 13$ to $t_1 = 16$, in discrete time. After $k = 16$, the instants of time are not considered candidate values of t_1 since the transport of the bar by drone 2 happens at $t_2 = t_1 + 3$. Thus, it is necessary to wait 3 samples after the instant t_1 for the transport of the bar to occur and 1 sample to observe its effects, in discrete time.

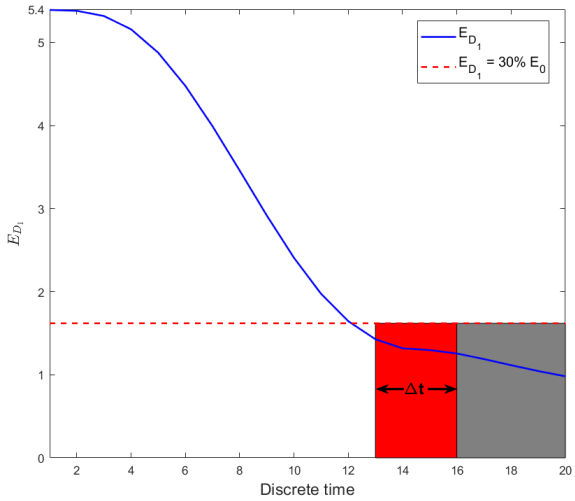

Figure 6.3: Choice of candidate values for t_1 present in Δt.

In the simulation shown in Fig. 6.4, the evolution of the total cost value, J_{total}, is represented for each candidate for t_1, ($t_1 = 13, 14, 15, 16$) in both cases. Note that when the dynamics of drone 1 is active, $J_{total} = J_1 + J_{opt_1}$ and when the second drone is active, $J_{total} = J_2 + J_{opt_2}$ The optimal switching time found for both cases is $t_1 = 1.6$ seconds, since J_{total} is minimal for that instant of time.

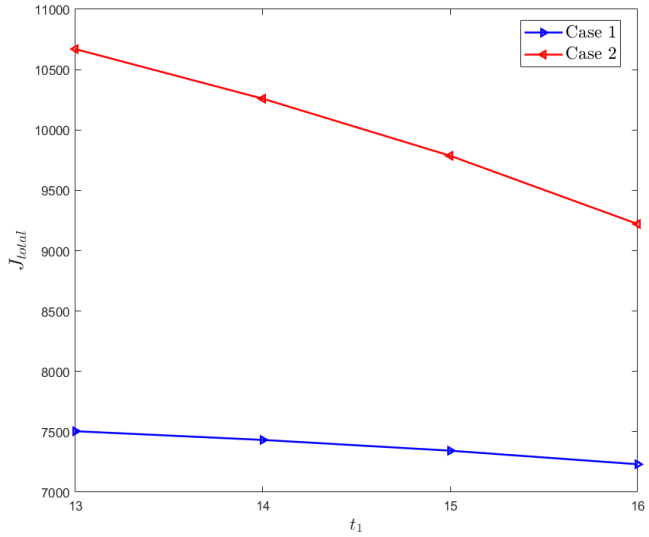

Figure 6.4: Total cost of both situations for $H = 26$ and $T_s = 0.1$.

Fig. 6.5 shows the energy consumption of the two vehicles for both scenarios. These two situations have four time periods in common, represented by gray circles, dictated by the behavior of drones.

1. Drone 1 is in motion, while drone 2 waits to intervene.
2. The beginning of this period marks the transition from dynamics 1 to the dynamics of the second vehicle. After this switch, which occurs at the optimum time t_1, only drone 2 is in motion.
   (a) During this time, drone 2 is in motion, without carrying the bar.
   (b) The initial moment of this interval, $t_2 = t_1 + 0.3$ seconds, marks the meeting of the drones. From this moment on, the second vehicle will carry the bar.

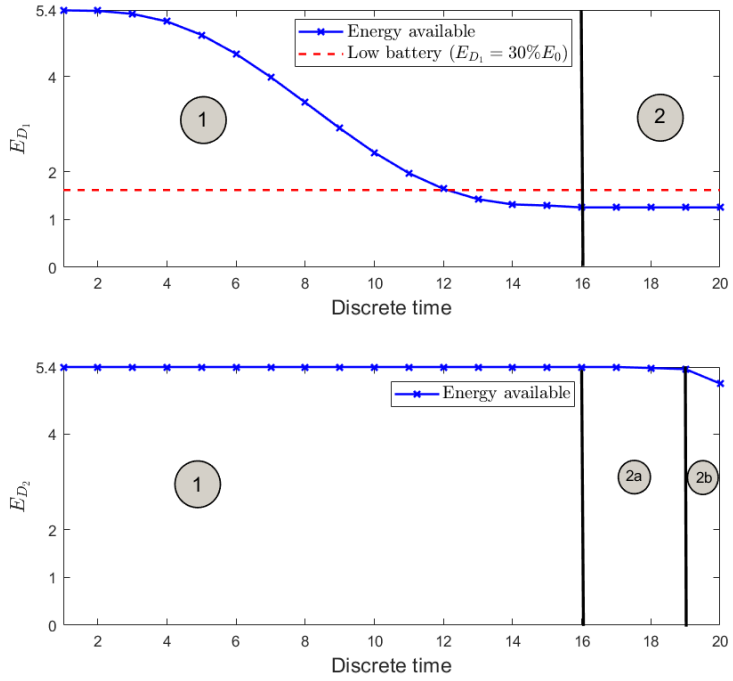

(a) Case 1

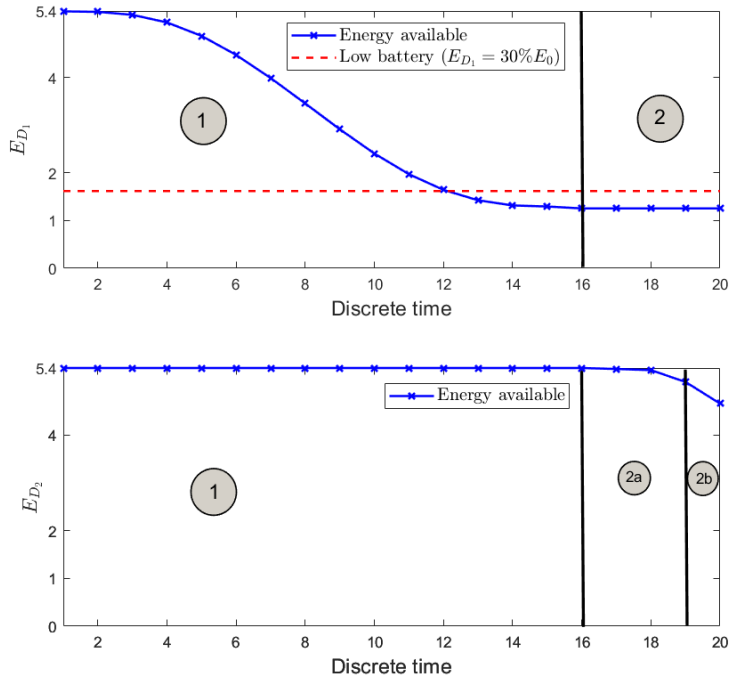

(b) Case 2

Figure 6.5: Vehicle energy consumption for both cases.

Impact of bar mass variation on drone 1 velocity

Fig. 6.6 shows the linear velocity of drone 1, $v_1 = \| \begin{bmatrix} v_{x_1} & v_{y_1} & v_{z_1} \end{bmatrix} \|$, as a function of the value of the mass of the bar. The values considered for the mass of the bar are $0.5\ kg$, $0.8\ kg$, $1\ kg$ and $1.2\ kg$, where the first value is the value adopted for case 1 and the last value depicts a situation in which the mass of the bar is greater than the mass of the vehicle that carries it.

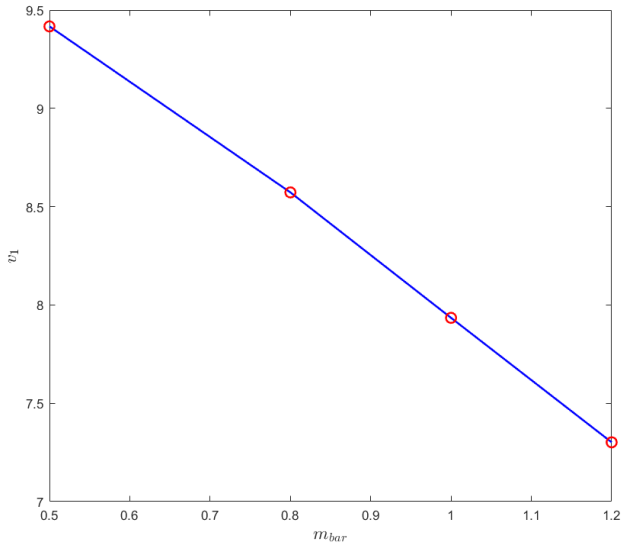

Figure 6.6: Linear velocity of drone 1 as a function of the mass of the bar.

Analyzing Fig. 6.6, it is concluded that, as expected, as the mass of the bar increases, the drone decelerates in order to manage its energy consumption, since the vehicle battery is finite ($0 < E_{C_1} < E_0$).

Impact of parameter Γ in E_{D_1}

As previously mentioned, the parameter Γ present in the cost functions J_{opt_1} and J_{opt_2} gives priority to minimizing the drone energy consumption when $\Gamma > 1$ and when $\Gamma < 1$, the main objective becomes to maximize the drone linear velocities.

In Fig. 6.7 is represented the energy available for drone 1, E_{D_1}, for case 1, for different values of Γ. It is concluded that, the higher the value of Γ, the greater importance is given to minimizing the energy of drone 1, as seen when $\Gamma = 2$. On the other hand, a small Γ value results in maximizing the linear velocities of drone 1, which is reflected in greater energy consumption by this vehicle.

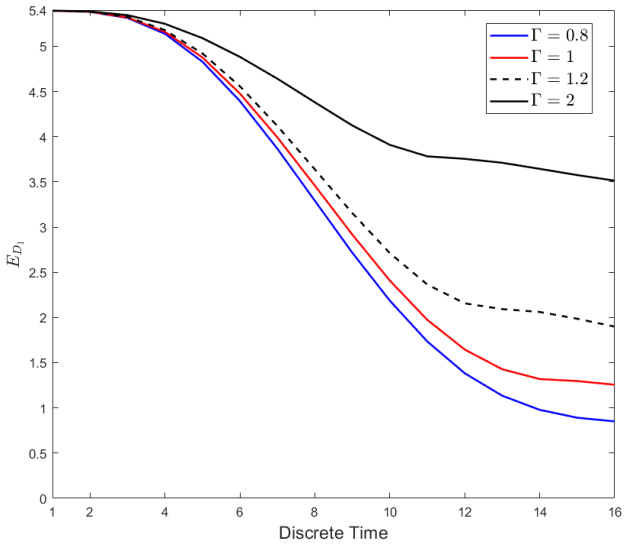

Figure 6.7: Energy available for drone 1, E_{D_1}, for different values of Γ.

Search for the optimal time t_2 with fixed time t_1

In the results obtained so far, it was assumed that the instant time when drone 2 departs from the base, t_1, varied and that the instant time when drone 2 starts to transport the bar, t_2, is fixed. Suppose now that t_1 is fixed and that t_2 varies. That is, for a fixed t_1, a search is performed in order to find the value Δ for which the sum of the 4 cost functions ($J_1 + J_{opt_1} + J_2 + J_{opt_2}$) is minimum. This search is summarized in the following expression

$$t_2 = t_1 + \Delta.$$

The search results in a set of data presented in a grid, shown in Table 6.2 for case 1 and in Table 6.3 for case 2, where the values of the sum of cost functions for the combination of the two instants, t_1 and t_2 are present, in the order of 10^4. In both tables, marked with a red rectangle, are the situations associated with the minimum value of the sum of the cost functions, for the combination of the two instant moments, t_1 and t_2.

Case 1

t_2 \ t_1	13	14	15	16
14	0.734	-	-	-
15	0.740	0.723	-	-
16	0.750	0.730	0.709	-
17	0.760	0.743	0.718	0.692
18	0.768	0.755	0.734	0.703
19	0.775	0.764	0.748	0.723

Table 6.2: Sum of cost functions for different combinations of t_1 and t_2, for case 1.

Case 2

t_2 \ t_1	13	14	15	16
14	1.053	-	-	-
15	1.057	1.009	-	-
16	1.067	1.012	0.957	-
17	1.077	1.026	0.962	0.894
18	1.085	1.038	0.979	0.901
19	1.093	1.048	0.99	0.922

Table 6.3: Sum of cost functions for different combinations of t_1 and t_2, for case 2.

As noted in Table 6.2 and in Table 6.3, the sum of cost functions is minimum for both cases for $(t_1, t_2) = (16, 17)$, which corresponds to a Δ equal to $\Delta = 1$, in discrete time.

That is, the optimal situation for the energy consumption of both drones is the dynamics of the second drone being activated from $t_1 = 16$ and the bar being transported at the first possible instant, $t_2 = t_1 + 1$, in discrete time. This situation is due to the fact that the later drone 2 meets with drone 1 to start transporting the bar, the greater the energy consumption of both vehicles.

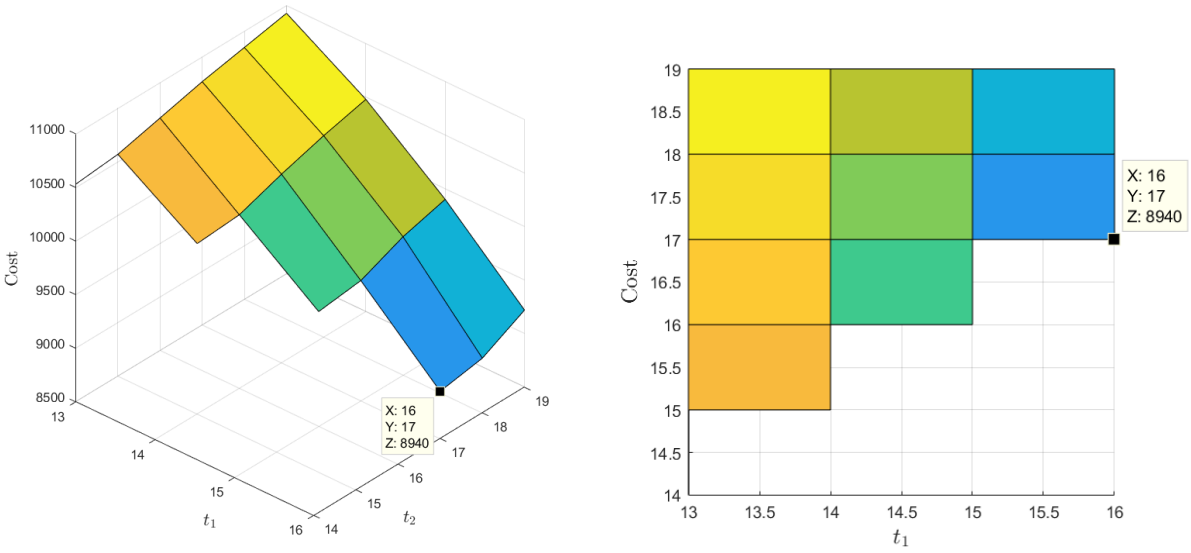

(a) 3D view

(b) Top view

Figure 6.8: 3D representation of the surface generated by the values defined for case 2.

Figure 6.8 shows the surface in three dimensions, generated through the values in Table 6.3, where it is observable that the sum of cost functions is minimal when $t_1 = 16$ and $t_2 = 17$, in discrete time.

Performance assessment of the controller

In order to assess the robustness of the controller developed for this system, several tests are carried out considering situations such as uncertainty in the model. In this section, all situations where non-idealities are present are compared to a reference situation: the state which represents the energy consumed by the first drone per unit of time, E_{C_1}, for case 1, where $m_1 = 0.5\ kg$. For the purpose of evaluating these situations, the following deviation measure is considered

$$\sigma_Y = \sqrt{\frac{1}{N}\sum_{i=1}^{N}(Y_i - \hat{Y}_i)^2}, \tag{6.13}$$

where Y_i is the vector of expected values, referring to the reference situation, $\hat{Y}_i$ is the vector of observed values and N is the total number of samples.

Unmodelled dynamics

There is noise in physical systems that is not possible to model, for example, the suspension of a car. In the case of the quadcopter model, there may be noise such as turbulence in the wind that is not possible to model, which is called process noise.

In this context, this section aims to introduce process noise, that is, unmodeled time-varying random disturbances, in the quadcopter model. The process noise is generated through a random binary sequence (a discrete-time stochastic process), represented by vector w. The dynamics of the vehicle now have an additional term and are given by

$$\begin{aligned}
\ddot{x}_1 &= \frac{T_1}{m_1}(\cos\psi_1 \sin\theta_1 \cos\phi_1 + \sin\psi_1 \sin\phi_1) + \textbf{w(1)},\\
\ddot{y}_1 &= \frac{T_1}{m_1}(\sin\psi_1 \sin\theta_1 \cos\phi_1 - \cos\psi_1 \sin\phi_1) + \textbf{w(2)},\\
\ddot{z}_1 &= -g + \frac{T_1}{m_1}(\cos\theta_1 \cos\phi_1) + \textbf{w(3)},\\
\dot{w}_{x_1} &= \frac{\tau_{x_1}}{I_{xx_1}} + w_{y_1} w_{z_1} \frac{I_{yy_1} - I_{zz_1}}{I_{xx_1}}, + \textbf{w(4)}\\
\dot{w}_{y_1} &= \frac{\tau_{y_1}}{I_{yy_1}} + w_{x_1} w_{z_1} \frac{I_{zz_1} - I_{xx_1}}{I_{yy_1}} + + \textbf{w(5)},\\
\dot{w}_{z_1} &= \frac{\tau_{z_1}}{I_{zz_1}} + w_{x_1} w_{y_1} \frac{I_{xx_1} - I_{yy_1}}{I_{zz_1}} + \textbf{w(6)},\\
\dot{E}_{C_1} &= K_1 \left| v_1^T \dot{v}_1 \right| + \left| w_1^T I_1 \dot{w}_1 \right| + \textbf{w(7)}.
\end{aligned} \tag{6.14}$$

Fig. 6.9 shows the simulation of state E_{D_1} in discrete time, where the reference situation is compared to the case in which there is process noise.

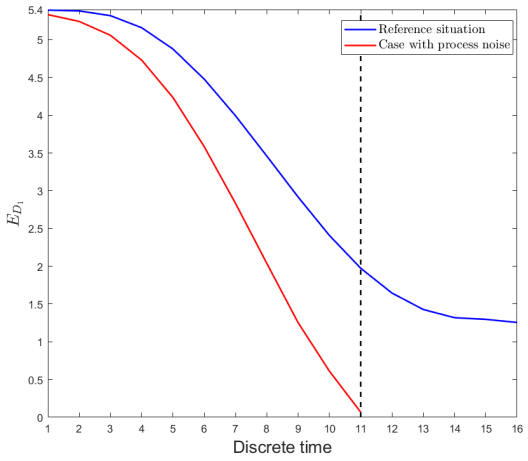

Figure 6.9: Comparison of the reference situation with the case in which there exists process noise.

As expected, the introduction of process noise causes a greater energy expenditure of drone 1. In fact, the drone does not reach the predetermined final position, despite having a restriction related to its battery, which is finite. In other words, when there is a process noise, the drone not only cannot finish the trajectory, but its consumed energy is not managed along the trajectory, as the restriction associated with the value of its battery is ignored.

It is worth noting that in this situation the fact that the drone has a maximum battery energy is beneficial because if this limit did not exist, errors would have to be promptly corrected, otherwise they would compound. In order to quantify the effect of process noise on this system, the deviation, σ_Y, between these two situations is calculated considering only the first 11 samples, resulting in $\sigma_Y = 1.15$.

Actuator dynamics

In this section, an analysis of the influence of actuator dynamics in the system is carried out. In the context of this work, the purpose of including actuator dynamics is to model how the quadcopter control varies with respect to the commanded control over time. Fig. 6.10 shows a diagram explaining the incorporation of the actuator dynamics in the system. In addition to the quadcopter states defined in chapter 3, there are now 4 new states: T_1, τ_{x_1}, τ_{y_1} and τ_{z_1}.

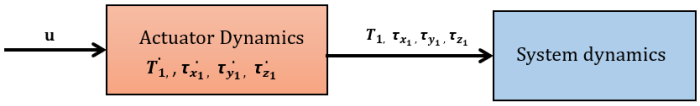

Figure 6.10: Explanatory scheme of the actuator dynamics.

As a simplification, it is considered that the dynamics of the actuators are represented by first order

equations, given by

$$\begin{aligned}
\dot{T_1} &= -\frac{1}{\tau_T}T_1 + \frac{1}{\tau_T}u_T, \\
\dot{\tau_{x_1}} &= -\frac{1}{\tau}\tau_{x_1} + \frac{1}{\tau}u_{\tau_x}, \\
\dot{\tau_{y_1}} &= -\frac{1}{\tau}\tau_{y_1} + \frac{1}{\tau}u_{\tau_y}, \\
\dot{\tau_{z_1}} &= -\frac{1}{\tau}\tau_{z_1} + \frac{1}{\tau}u_{\tau_z},
\end{aligned} \tag{6.15}$$

where u_T is the actuation command for the total thrust force exerted on drone 1, T_1, and u_{τ_x}, u_{τ_y} and u_{τ_z}, are, respectively, the actuation commands for the drone rolling, pitching and yawning moments. Additionally, τ_T and τ represent the time constants that characterizes the response speed of the actuator for T_1 and for τ_{x_1}, τ_{y_1} and τ_{z_1}, respectively. The values defined for the time constants present in this simulation are $\tau_T = 5 \cdot 10^{-2} s$ and $\tau = 4 \cdot 10^{-2}\ s$.

In Fig. 6.11, E_{D_1} is represented for a situation in which there is actuator dynamics and for a situation in which there is no actuator dynamics. It is observed that there is a higher energy expenditure for the first case, which results indirectly from the calculation of the control that will later affect the states of the drone model, such as E_2.

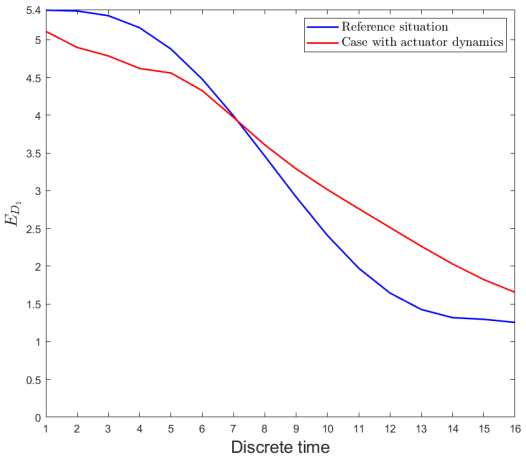

Figure 6.11: Comparison of the reference situation with a situation in which there exists actuator dynamics.

In Fig. 6.12, the time evolution of the states T_1, τ_{x_1}, τ_{y_1} and τ_{z_1} is represented. Note that τ_{z_1} takes a value close to 0 because the drone does not accelerate in the z direction. The impact of including the actuator dynamics in this example is calculated through the deviation measure, whose value is $\sigma_Y = 0.53$.

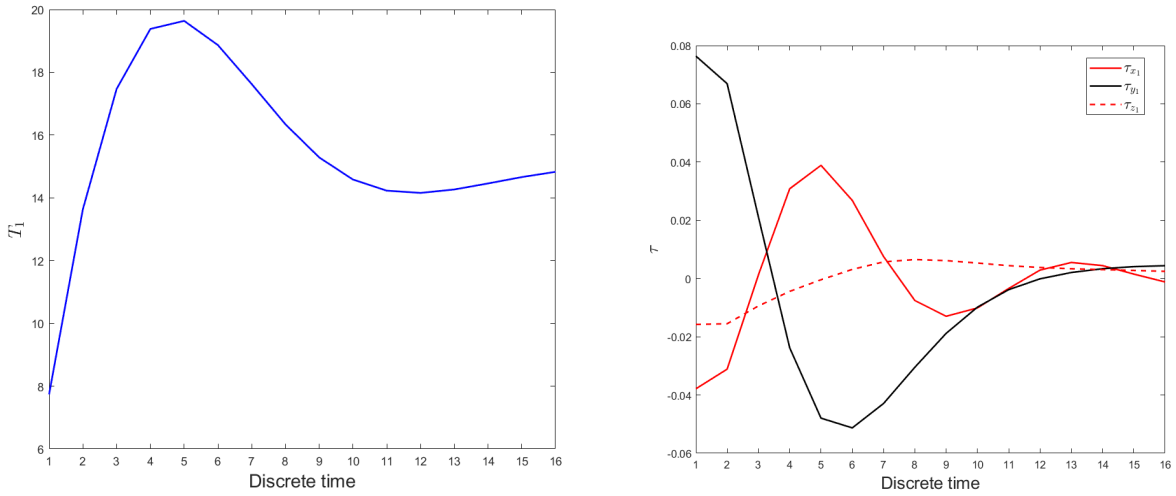

(a) State T_1.

(b) States τ_{x_1},τ_{y_1} and τ_{z_1}.

Figure 6.12: Time evolution of states T_1, τ_{x_1}, τ_{y_1} and τ_{z_1}.

In conclusion, of all the situations represented, the one who considered process noise had the most negative impact on the system, causing higher energy consumption by the vehicle, reflected in the shortened flight time of the drone, when compared to a situation where there is no process noise. The high value of σ_Y is justified by the fact that the process noise directly impacts the dynamics of the entire system.

Finally, the inclusion of the actuator dynamics caused a lesser negative impact on the system, revealing lower energy consumption, even though this situation directly affects the control of the system. It is important to note that the ideal adjustment of the time constants will always reveal a more optimal energy consumption scenario. Additionally, although the actuator dynamics first order equation serves the context considered here, this choice causes a simplification in the optimization problem, which directly impacts all optimization variables present in the model.

Chapter 7

Conclusions

In this Chapter, a review of the work is done and conclusions are drawn. In addition, recommendations are made for research paths, based on the problems addressed in this dissertation.

The objective of this dissertation was to develop a controller in order to solve the problem of transporting large objects by a multi-drone system. This purpose was achieved through a strategy based on nonlinear predictive control algorithms. Additionally, the problem of performing missions with a duration that goes beyond the autonomy of a single drone in a multi-drone system was considered. The solution to this problem took into account the aforementioned non-linear MPC technique and also a pseudo-algorithm of searching for the optimum instant of the departure of a second vehicle from the base so that the replacement of the vehicle occurs.

At the beginning of Chapter 3, the bi-rotor model was studied, whose knowledge was then applied to the analysis of a more complex system, composed of two bi-rotors that carry a bar. In both systems, the dynamics were defined using the Euler-Lagrange equations. Subsequently, the quadcopter model was defined and this knowledge was applied to the study of a problem with greater complexity: the modeling of a system composed of two drones that cooperate in order to transport a bar. For this system, it was considered a different configuration from the usual one, where the bar is connected to each drone through spherical joints, which allows the total mobility of both vehicles. In Chapter 4, the control strategy for the bi-rotor bar system was analyzed, where simulations were performed in order to analyze the robustness of the controller developed for this system. Additionally, an evaluation of the performance of the system was carried out, through the variation of the following parameters: the prediction horizon, H, the sampling time, T_s, and the weight β applied to the total thrust force of both vehicles.

In Chapter 5, the control of the quadcopter bar system was carried out, where simulations for different maneuvers to be performed by the system were presented.

Chapter 6 was dedicated to the problem of vehicle replacement. In this context, it was assumed that each vehicle was able to transport the bar individually. The problem was formulated in the following

way: It was considered that a drone would depart from a given position in order to transport the bar to a defined final position. However, this vehicle did not have enough energy to complete the predefined trajectory. Thus, the need arose to introduce another UAV so that, when the drone 1 available energy was below or equal to 30%, ($E_{D_1} \leq 0.3E_0$), the second drone could depart from the base and meet his peer, in order to finish the rest of the trajectory, carrying the bar.

In this problem, two possible scenarios were considered: a first case where both drones were symmetrical and identical and another case where the second vehicle presented such an asymmetry in relation to the first one, which caused the transport of the bar to add an energy expense of 90% to its energy consumption rate. To address this situation, an energy consumption model was defined for each drone, which introduced a new state, E_{C_i}, that represents the energy consumption of each vehicle i ($i = 1, 2$). Taking into account this model, it was possible to search for the optimum instant, t_1, from which the second dynamics would be activated. It should be remembered that t_1 belonged to a range of candidates present in a time interval that was defined taking into account the instants of time when the energy available of drone 1 was equal to or less than 30%. Thus, an interval search algorithm was defined, based on the minimum cost for each instant of time, in order to find the optimal instant, t_1. For the two cases, the same value of t_1 was obtained.

Finally, a study of the robustness of the controller was made, where uncertainty in the model was considered through through the inclusion of actuator dynamics and process noise.

In conclusion, predictive control is a powerful tool due to its ability to allow the incorporation of restrictions into optimization problems. It is possible to solve problems of increasing complexity such as the transport problem carried out through the cooperation of two quadcopters, presented in this work. However, it is often necessary to resort to simplifications of the problem as it was also done in the modeling and control of this system, in order to avoid very high computation times. Therefore, a compromise between the complexity of the problem to be addressed and the added computational burden of the problem must be taken into account. It should also be noted that the problem of the drone autonomy can be analyzed with much greater depth, considering, for example, more than one active dynamics at the same time.

7.1 Future Work

There are several research paths that can be followed, based on this dissertation.

On the one hand, the problem of transporting large objects by a multi-drone system can be explored through the proposal of a decentralized control approach. That is, each drone would have an associated MPC controller and, for that purpose, there would be as many optimization problems to solve as the number of drones present in the system. Additionally, vehicles would exchange data with their peers. This would be an efficient solution to allow more drones to be included in the system, without compromising its performance. Note that, even if there was a problem with a vehicle controller that forced it to stop, the multi-drone system would not necessarily need to stop its ongoing mission.

On the other hand, a more sophisticated approach to the problem of vehicle replacement could be

considered. For example, a distributed strategy could be implemented so that drones could communicate via commands or messages, and possibly provide a decentralized and scalable solution, robust to partial system failures.

Appendices

Appendix A

Experimental setup

The previous chapter dealt with system modeling, considering different aspects of system design. This chapter aims to show the resources used to implement the control of the two multi-drones systems presented in this work.

A.1 Software

The nonlinear predictive controller developed in this work was implemented using MATLAB (ver. R2018a) and some of its built-in functions, such as the optimization Toolbox fmincon function and solver ode45, analyzed below.

A.1.1 Fmincon Solver

Matlab has several solvers that can be used to solve certain optimization problems, based on its characteristics. In the context of this work, the chosen solver was fmincon, because, when initial conditions and the solver options are properly chosen, it can find the local minimum value of a nonlinear multivariable function taking into account constraints to the problem, whether linear or nonlinear.

Thus, fmincon finds the minimum value of functions with the following form [21]

$$\begin{aligned} &\underset{x}{\text{minimize}} \quad f(x) \\ &\text{subject to} \\ &\qquad c(x) \leq 0, \\ &\qquad ceq(x) = 0 \\ &\qquad A \cdot x \leq b, \\ &\qquad Aeq \cdot x = Beq, \\ &\qquad lb \leq x \leq ub, \end{aligned} \tag{A.1}$$

where x corresponds to the optimization variables (scalar or vector), $f(x)$ corresponds to the cost func-

tion to be minimized, which is constructed taking these variables into account and lb and ub correspond, respectively, to the lower and upper bounds of x.

As for the restrictions, these can be linear or non-linear. $Aeq \cdot x = Beq$ and $A \cdot x \leq b$ represent, respectively, the linear equalities and linear inequalities and the first two constraints present in (A.1), represent the non-linear equalities and nonlinear inequalities of the optimization problem.

In terms of the actual implementation of fmincon in MATLAB, the solver has the following synthax, where options can be specified for its optimization

```
x = fmincon(fun,x0,A,b,Aeq,beq,lb,ub,nonlcon,options)
options = optimoptions('fmincon','Algorithm','sqp','TolFun'
,0.001,'MaxIter',10000,'MaxFunEvals',10000);
```

To carry out its implementation, the solver has five algorithm options:

1. interior-point (default)
2. trust-region-reflective
3. sqp
4. sqp-legacy
5. active-set

For the development of the NMPC controller considered in this work, the sequential quadratic programming (sqp) algorithm was considered since it is a class of algorithms that can handle non-linearities, proving to be adequate when implementing the controller, resulting in a feasible solution. However, depending on the optimization problem at hand and its implementation, another algorithm could have been considered.

In this context, fmincon works as follows: based on the sequential quadratic programming algorithm and given an initial starting point, the solver outputs a local optimum solution vector for the problem.

Note that, to use this solver, the following situations must be taken into account

1. Fmincon is a local solver, which means that this general minimization solver follows gradient descent and so it can get ”trapped” in a local minimum value that is not necessarily the optimal one.
2. Fmincon requires a high speed processor in order to return a timely solution to complex problems like the one presented in this work.

A.1.2 Solver ode45

Allied to fmincon, the solver ode45 is considered in order to formulate the system model, which considers differential equations. In the following two chapters, in the optimization problems considered, the cost function is defined in discrete time and the system constraints (corresponding to the system dynamics)

are defined in continuous time since the use of this solver eliminates the need to discretize the system dynamics equations.

Thus, ode45 solves system of differential equations of the form

$$y' = f(t, y),$$

where y corresponds to the the optimization variables vector and t corresponds to a time vector. Additionally, this solver has the following syntax [22]

```
[t,y] = ode45(odefun,tspan,y0)
```

where $odefun$ corresponds to the function to be solved, $tspan$ corresponds to the time interval in which the integration of the system is done and $y0$ corresponds to the vector of initial conditions.

Bibliography

[1] S. Lupashin, A. Schöllig, M. Sherback and R. D'Andrea, "A simple learning strategy for high-speed quadrocopter multi-flips", *2010 IEEE International Conference on Robotics and Automation*, pp. 1642-1648, 2010.

[2] S. Waslander, *ME597: Autonomous Mobile robotics, section 2- coordinate transforms*, University of Waterloo, 2008.

[3] T. Kusznir and J. Smoczek, "Sliding Mode-Based Control of a UAV Quadrotor for Suppressing the Cable-Suspended Payload Vibration", *Journal of Control Science and Engineering*, vol.2020, pp. 1-12, 2020.

[4] Z. Wang, S. Singh, M. Pavone and M. Schwager, "Cooperative Object Transport in 3D with Multiple Quadrotors Using No Peer Communication", *2018 IEEE International Conference on Robotics and Automation (ICRA)*, pp. 1064-1071, 2018.

[5] R. Praveen Jain, "Transportation of cable suspended load using unmanned aerial vehicles: A real-time model predictive control approach", *Msc Thesis*, Delft University of Technology, 2015.

[6] A. Das and V. Sharma, "Modelling of uncertainty in control systems and design of a robust controller using H_∞ method", *2017 International Conference on Intelligent Computing and Control Systems (ICICCS)*, pp. 1008-1013, 2017.

[7] C. Masone, H. H. Bülthoff and P. Stegagno, "Cooperative transportation of a payload using quadrotors: A reconfigurable cable-driven parallel robot," *2016 IEEE/RSJ International Conference on Intelligent Robots and Systems (IROS)*, pp. 1623-1630, 2016.

[8] L. Ha, D. Bui and S. Hong, "Nonlinear Control for Autonomous Trajectory Tracking While Considering Collision Avoidance of UAVs Based on Geometric Relations," *Multidisciplinary Digital Publishing Institute* , vol. 12, pp.1551, 2019.

[9] M. Erdelj, O. Saif, E. Natalizio and I. Fantoni, "UAVs that Fly Forever: Uninterrupted Structural Inspection through Automatic UAV Replacement", *Ad Hoc Networks*, vol. 94, December 2017.

[10] J. Zhang, J. Campbell, D. Sweeney and A. Hupman, "Energy Consumption Models for Delivery Drones: A Comparison and Assessment", *Project: Drone Delivery*, University of Missouri-St. Louis, May 2020.

[11] M. Alamir and S. Attia, ”On solving optimal control problems for switched hybrid nonlinear systems by strong variations algorithms”, *Laboratoire d'Automatique de Grenoble, Domaine Universitaire*, 2003.

[12] European Comission, ”Digital Transformation Monitor - Drones in Agriculture”, January 2018.

[13] P. R. Grammatikis, P. G. Sarigiannidis, T. Lagkas, Thomas and I. Moscholios, ”A Compilation of UAV Applications for Precision Agriculture”, *Computer Networks*, vol.172, pp. 107-148, February 2020.

[14] R. Bonatti, W. Wang, C. Ho, A. Ahuja, M. Gschwindt, E. Camci, E. Kayacan, S.Choudhury and S. Scherer, ”Autonomous aerial cinematography in unstructured environments with learned artistic decision-making”, *Journal of Field Robotics*, vol.37, January 2020.

[15] Y. Wang, F. Xu and V. Puig, ”Nonlinear Model Predictive Control with Constraint Satisfactions for a Quadcopter”, *Journal of Physics: Conference Series*, vol.783, 2016.

[16] R. P. L. Jain, ”Transportation of Cable Suspended Load using Unmanned Aerial Vehicles - A Real-time Model Predictive Control Approach”, Msc Thesis, Delft University of Technology, 2016.

[17] A. Torres-González, J. Capitán, R. Cunha, A. Ollero and I. Mademlis, ”A Multidrone Approach for Autonomous Cinematography Planning”, *Advances in Intelligent Systems and Computing*, pp.337-349, 2018.

[18] Z. Wang, S. Singh, M. Pavone and M. Schwager, ”Cooperative Object Transport in 3D with Multiple Quadrotors Using No Peer Communication”, *International Conference on Robotics and Automation*, pp. 1064-1071, 2018.

[19] Chris Bretherton, ”Lecture 11: White and red noise”, Computational Methods for Data Analysis, University of Washington, Winter 2014.

[20] S. Boyd and L. Vandenberghe, ”Lecture: Convex Optimization”, Convex Optimization I, Stanford University, 2004

[21] fmincon, “fmincon.” [Online]. Available: `https://www.mathworks.com/help/optim/ug/fmincon.html`.

[22] ode45, “ode45.” [Online]. Available: `https://www.mathworks.com/help/matlab/ref/ode45.html`.